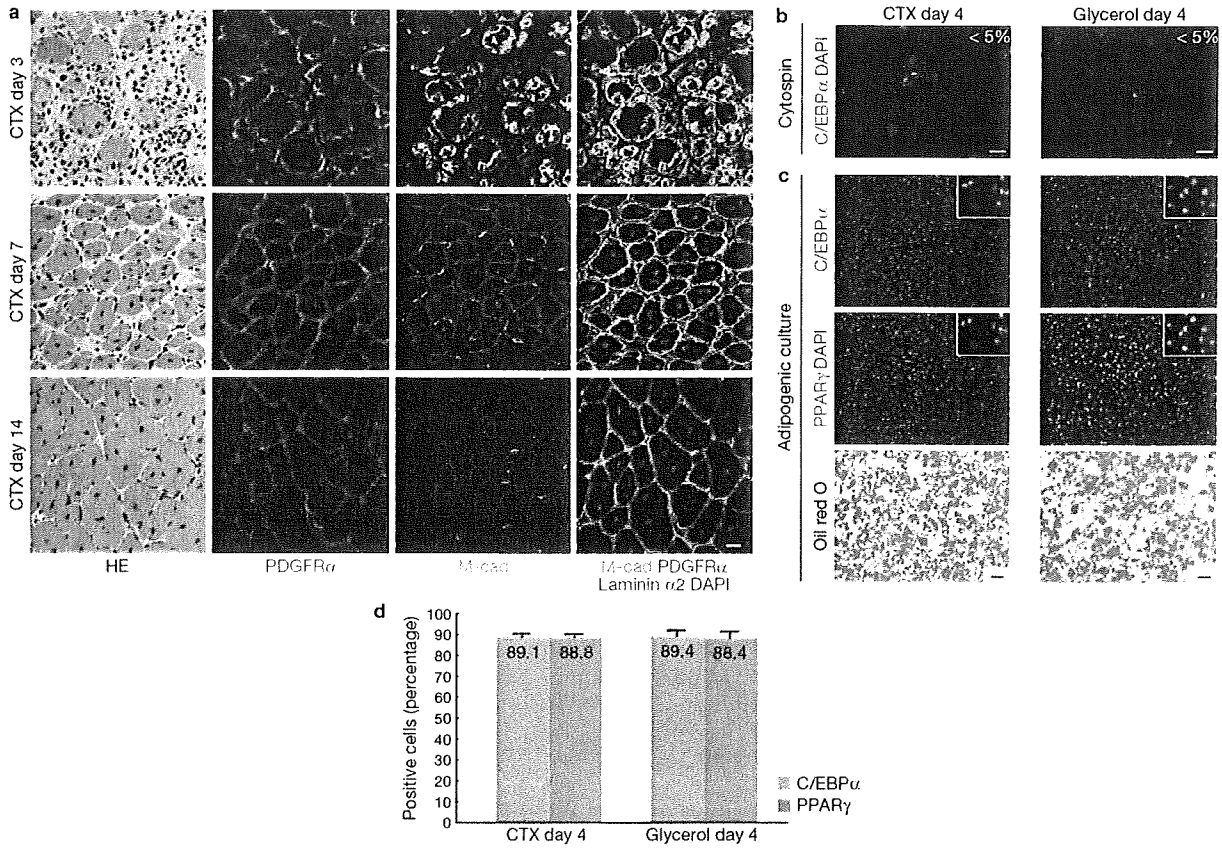

Figure 6 The behaviour of PDGFRα⁺ cells during CTX-induced muscle regeneration and adipogenic potentials of PDGFRα⁺ cells isolated from regenerating or degenerating muscle. (**a**) At the indicated time points after CTX injection, muscle sections were subjected to immunofluorescence staining for M-cadherin (M-cad), PDGFRα and laminin α2 before hematoxylin and eosin (HE) staining. (**b**) Four days after CTX or glycerol injection, CD31⁻CD45⁻PDGFRα⁺ cells were isolated from treated muscles and subjected to cytospin and then analysed for C/EBPα expression. The values in the top panels represent the percentages of positive cells. (**c**) CD31⁻CD45⁻PDGFRα⁺ cells isolated from CTX or glycerol-injected muscles were cultured under adipogenic conditions. Adipogenic differentiation was revealed by immunofluorescence staining for C/EBPα and PPARγ or by oil red O staining. (**d**) Adipogenic differentiation was evaluated by quantifying the percentages of C/EBPα- and PPARγ-positive cells. Error bars indicate the mean ± s.d., $n = 15$ fields pulled out from three independent experiments. Scale bars, 20 μm (**a**) 30 μm (**b**) and 50 μm (**c**).

in the regeneration of glycerol-injected muscles could be attributed to impaired proliferation of Pax7⁺ myogenic progenitors at an earlier stage (Supplementary Information, Fig. S10). At day 14, in the CTX model, regenerated myofibres with central nuclei were located throughout the tibialis anterior muscles and adipocytes were rare (Fig. 8f–f‴, h). In contrast, glycerol-injected muscle had fewer regenerated myofibres, and ectopic adipocytes as well as necrotic fibres occupied a considerable area of the muscles (Fig. 8g–g‴, h). These results suggest that interaction between regenerating myofibres and PDGFRα⁺ cells may be important for the inhibition of ectopic fat formation. To examine the effect of interaction between myofibres and PDGFRα⁺ cells, GFP⁺PDGFRα⁺ cells were co-cultured with wild-type satellite cells. In marked contrast to a single culture, adipogenic differentiation of PDGFRα⁺ cells was dramatically inhibited in co-culture (Fig. 8i, j). GFP⁺ cells occupied spaces between GFP⁻ satellite cell-derived myotubes, and most of them were negative for adipogenic markers (Fig. 8j). GFP⁺ adipocytes expressing C/EBPα and PPARγ were only rarely observed in co-culture (Fig. 8j, l). These results suggest that satellite cell-derived muscle fibres generate factors that strongly inhibit adipogenic differentiation of PDGFRα⁺ cells. To investigate whether such factors are produced in soluble forms, we generated conditioned cultures. Satellite cells were treated with adipogenic induction medium for 1 day. During this conditioning period, satellite cells rapidly differentiated and formed large myotubes (data not shown). Therefore, soluble factors produced by differentiating myoblasts or differentiated myotubes should have been present in the culture supernatant. When this conditioned medium was applied to the solo culture of PDGFRα⁺ cells, we could not see any inhibitory effects on adipogenic differentiation (Fig. 8k, l). In a transwell co-culture where PDGFRα⁺ cells and satellite cells were separated by a culture insert with 1.0-μm pore, inhibition of PDGFRα⁺ cell-dependent adipogenesis was not observed (data not shown). Taken together, our results suggest that satellite cell-derived muscle fibres exert an inhibitory effect on the adipogenesis of PDGFRα⁺ cells by directly interacting with them.

DISCUSSION

In this study, we identified mesenchymal progenitors in skeletal muscle using PDGFRα as a marker. PDGFRα is known to be expressed in mesenchymal cells. Particularly strong expression of PDGFRα has been observed in subtypes of mesenchymal progenitor cells and oligodendrocyte progenitors,

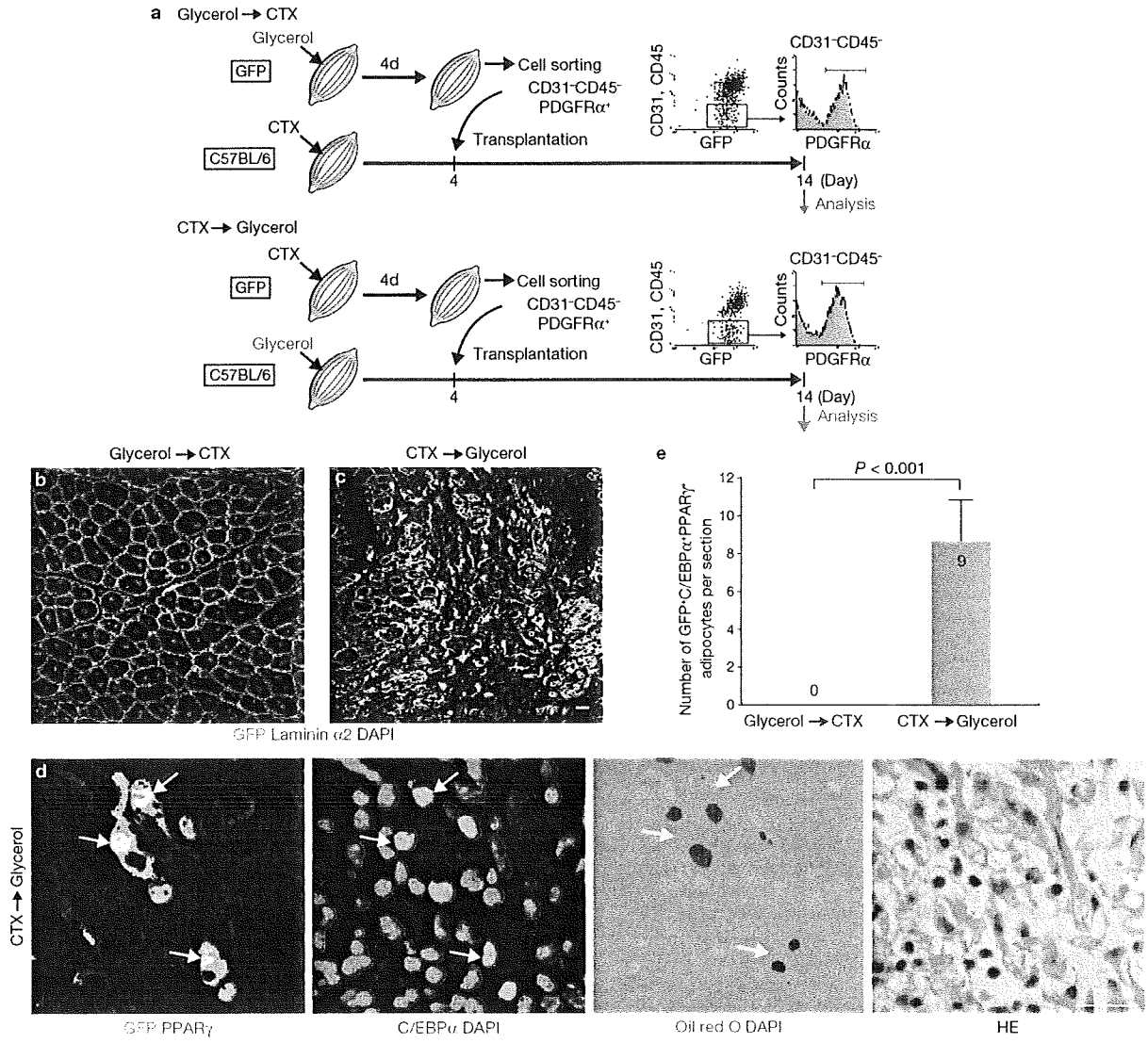

Figure 7 The fate of PDGFRα⁺ cells is largely dependent on the muscle environment. (**a**) Reciprocal transplantation procedures. (**b**, **c**) Two weeks after transplantation, the transplanted muscles were analysed for expression of GFP and laminin α2. (**d**) Adipogenic differentiation of transplanted cells was revealed by immunofluorescence staining for GFP, C/EBPα and PPARγ, and subsequent oil red O staining followed by hematoxylin and eosin (HE) staining. Arrows indicate GFP⁺C/EBPα⁺PPARγ⁺ oil red O⁺ unilocular adipocytes. (**e**) Quantitative analysis of reciprocal transplantation experiments. Error bar indicates the mean ± s.d., $n = 6$ in each group.

and PDGF-A–PDGFRα signalling appears to regulate a broad range of progenitor cells in several developmental processes[23]. During somitogenesis, PDGFRα is initially expressed throughout the undifferentiated somite and later becomes progressively restricted to the sclerotome and to a lesser extent the dermatome, but its expression disappears in the myotome as differentiation of the somite proceeds[24]. In a previous study, paraxial mesodermal progenitors were isolated from *Pax3*-induced embryoid bodies using PDGFRα as a positive selection marker, however, this receptor was downregulated in the derivative myogenic cells[25]. Thus, it seems that early mesodermal progenitors lose PDGFRα expression when they differentiate into the myogenic lineage. Recently, PDGFRα⁺ cells have been isolated from mouse bone marrow and characterized as a population highly enriched for MSCs[26–28]. Both PDGFRα and PDGFRβ are expressed in MSCs, but MSCs have a higher cell surface PDGFRα:PDGFRβ ratio than the differentiated cell type, and abundant PDGFRα appears to be a characteristic of undifferentiated MSCs[29]. Similarly, we observed downregulation of PDGFRα after adipogenic differentiation of muscle mesenchymal progenitors. Taken together, these results indicate that PDGFRα is an excellent marker for stem or progenitor cells of mesenchymal lineages.

Adipocyte progenitor cells have been previously identified in white adipose tissue using a FACS-based cell isolation method[30]. Interestingly, the white adipose tissue progenitors and mesenchymal progenitors in muscle reported here have a similar cell-surface phenotype ($CD31^-CD45^-CD29^+CD34^+Sca\text{-}1^+$), raising the possibility that progenitors with common cell-surface phenotypes may be isolated from diverse tissues.

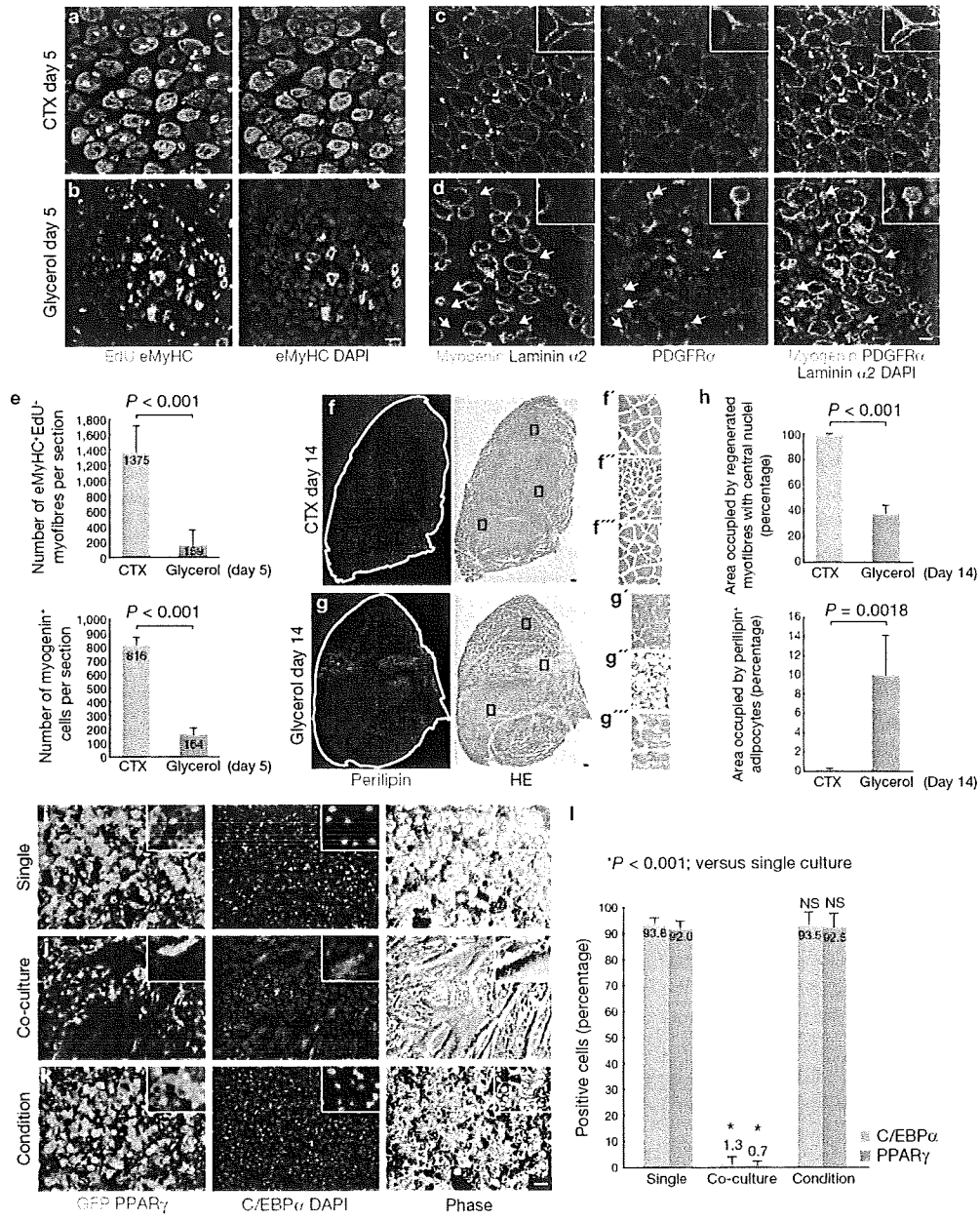

Figure 8 Satellite cell-derived myofibres inhibit adipogenic differentiation of PDGFRα⁺ cells. (**a**, **b**) EdU was administered 2, 3 and 4 days after CTX (**a**) or glycerol (**b**) injection. Five days after injury, muscle sections were subjected to eMyHC staining followed by EdU detection. (**c**, **d**) Expression of myogenin, PDGFRα and laminin α2 at day 5 after CTX (**c**) or glycerol (**d**) injection. Arrows indicate PDGFRα⁺ cells that lost physical interaction with myofibres and showed a morphological change in glycerol-injected muscle. Insets show high magnification images. (**e**) Quantitative analysis of eMyHC⁺EdU⁺ myofibres ($n = 6$ in each group) and myogenin⁺ cells ($n = 4$ in each group). Error bars indicate the mean ± s.d. (**f**–**g‴**) Muscle sections were subjected to perilipin staining followed by hematoxylin and eosin (HE) staining 14 days after injury. High magnification images of rectangular regions in **f** and **g** are shown in **f′**–**f‴** and **g′**–**g‴**, respectively. Glycerol-injected muscle had large areas occupied by adipocytes (**g″**) or necrotic fibres (**g‴**). (**h**) Quantitative analysis of regenerated area and fatty degenerated area. Error bars indicate mean ± s.d., $n = 4$ in the CTX group and $n = 5$ in the glycerol group. (**i**–**k**) CD31⁻CD45⁻SM/C-2.6⁻PDGFRα⁺ cells isolated from GFP Tg mice were cultured with or without wild-type CD31⁻CD45⁻SM/C-2.6⁺ cells. Cultures were treated with adipogenic medium or satellite cell-conditioned medium. Adipogenic differentiation was revealed by immunofluorescence staining for GFP, C/EBPα and PPARγ. (**l**) Adipogenic differentiation was evaluated by quantifying the percentages of C/EBPα- and PPARγ-positive GFP⁺ cells. Error bars indicate the mean ± s.d., $n = 15$ (single and condition cultures) or 20 (co-cultures) fields pulled from three independent experiments. NS, not significant. Scale bars, 20 μm (**a**–**d**), 100 μm (**f**, **g**) and 50 μm (**i**–**k**).

The physiological roles of PDGFRα⁺ mesenchymal progenitors remain to be elucidated. However, they may provide a supporting function for the muscle, as they encircle the sheath of muscle basement membrane in which satellite cells undergo active myogenesis during muscle regeneration (Fig. 6a). Interestingly, CD90⁺ fibroblast-like cells in skeletal muscle produce the muscle basement membrane component

laminin α2 (ref. 31), and PDGFRα⁺ and CD90⁺ cells are nearly identical (Supplementary Information, Fig. S1a). Thus, PDGFRα⁺ cells may have positive roles in muscle regeneration in part by producing basement membrane that functions as a scaffold for efficient myogenesis.

This study highlights the importance of PDGFRα⁺ mesenchymal progenitors in the context of ectopic fat formation in skeletal muscle. In obesity and various myopathies, fat accumulation is known to be more conspicuous in perimysium, particularly in perivascular space[2,5], where PDGFRα⁺ cells are commonly observed (Fig. 3e). One of the most intriguing results of our study is that factor(s) from satellite cell-derived myofibres strongly inhibited adipogenesis of PDGFRα⁺ cells. Thus, it seems that the balance between satellite cell-dependent myogenesis and PDGFRα⁺ cell-dependent adipogenesis, rather than multipotency of satellite cells, has a considerable impact on muscle homeostasis. As ectopic adipocytes usually arise under disease conditions where there has been destruction of muscle fibres without efficient regeneration[3], the model in which myofibres themselves have an inhibitory effect on the adipogenesis of PDGFRα⁺ cells makes sense. However, there are cases where our model would not apply, including obesity and type II diabetes[4,5], as there is no apparent muscle destruction in such diseases. In these conditions, systemic factors may have a role in the regulation of the adipogenesis of PDGFRα⁺ cells. In fact, we used high glucose medium containing several pro-adipogenic inducers for *in vitro* adipogenic differentiation. Additional experiments revealed that IBMX and dexamethasone are unnecessary, but insulin is required for efficient adipogenic differentiation of PDGFRα⁺ cells (data not shown). Furthermore, a high glucose condition is reported to enhance adipogenic differentiation of muscle-derived cells[32]. Thus, it is possible that systemic factors such as hormonal level or nutrition status may exert a stimulatory influence on the adipogenesis of PDGFRα⁺ cells. Overall, the fate of PDGFRα⁺ cells can be influenced by several aspects of the environment, and the balance between positive and negative factors may determine the final outcome.

In conclusion, we report the identification of PDGFRα⁺ mesenchymal progenitors that contribute to adipogenesis in skeletal muscle, and demonstrate a possible role for myofibres in regulating the fate of PDGFRα⁺ cells. We suggest that these cells are responsible for ectopic fat cell formation within skeletal muscle in pathological conditions such as DMD, denervation, obesity and ageing-related sarcopenia. Targeting PDGFRα⁺ mesenchymal progenitors may open new opportunities for designing therapeutic strategies to treat muscle diseases. □

METHODS

Methods and any associated references are available in the online version of the paper at http://www.nature.com/naturecellbiology/.

Note: Supplementary Information is available on the Nature Cell Biology website.

ACKNOWLEDGEMENTS

We thank S. Miura, M. Nakatani and T. Sato for technical assistance, F. Rossi for providing DyLight 649-conjugated rat anti-integrin α7, A. Miyajima for providing a rat anti-Dlk1 antibody and N. Hashimoto for providing a rabbit anti-myogenin antibody. This work was supported by JSPS KAKENHI (18890216; to A.U.), MEXT KAKENHI (21790884; to A.U.), a research grant (H20-018) on psychiatric and neurological diseases and mental health and a research grant (20B-13) for nervous and mental disorders from the Ministry of Health, Labour and Welfare.

AUTHOR CONTRIBUTIONS

A.U. was responsible for designing and performing the experiments, analysing the data and writing the manuscript; S.F. performed BM-transplantation and provided reagents; A.U. performed FACS experiment with help from N.Y.; S.T. provided reagents and materials and A.U. and K.T. coordinated the whole project.

COMPETING FINANCIAL INTERESTS

The authors declare no competing financial interests.

Published online at http://www.nature.com/naturecellbiology/.
Reprints and permissions information is available online at http://npg.nature.com/reprintsandpermissions/.

1. Bischoff, R. Satellite and stem cells in muscle regeneration, in *Myology*, Vol. 1, Edn. 3. (eds. A. G. Engel & C. Franzini-Armstrong) 66–86 (McGraw-Hill, New York; 2004).
2. Banker, B. Q. & Engel, A. G. Basic reactions of muscle, in *Myology*, Vol. 1, Edn. 3. (eds. A. G. Engel & C. Franzini-Armstrong) 691–747 (McGraw-Hill, New York; 2004).
3. Carpenter, S. & Karpati, G. Cells and structures other than skeletal muscle fibers, in *Pathology of skeletal muscle*, Edn. 2 314–369 (Oxford, New York; 2001).
4. Goodpaster, B. H. & Wolf, D. Skeletal muscle lipid accumulation in obesity, insulin resistance, and type 2 diabetes. *Pediatr. Diabetes* **5**, 219–226 (2004).
5. Greco, A. V. *et al.* Insulin resistance in morbid obesity: reversal with intramyocellular fat depletion. *Diabetes* **51**, 144–151 (2002).
6. Visser, M. *et al.* Muscle mass, muscle strength, and muscle fat infiltration as predictors of incident mobility limitations in well-functioning older persons. *J. Gerontol. A Biol. Sci. Med. Sci.* **60**, 324–333 (2005).
7. Rosen, E. D. & Macdougald, O. A. Adipocyte differentiation from the inside out. *Nature Rev. Mol. Cell Biol.* **7**, 885–896 (2006).
8. Gregoire, F. M., Smas, C. M. & Sul, H. S. Understanding adipocyte differentiation. *Physiol. Rev.* **78**, 783–809 (1998).
9. Linhart, H. G. *et al.* C/EBPα is required for differentiation of white, but not brown, adipose tissue. *Proc. Natl Acad. Sci. USA* **98**, 12532–12537 (2001).
10. Tontonoz, P., Hu, E. & Spiegelman, B. M. Stimulation of adipogenesis in fibroblasts by PPARγ 2, a lipid-activated transcription factor. *Cell* **79**, 1147–1156 (1994).
11. Asakura, A., Komaki, M. & Rudnicki, M. Muscle satellite cells are multipotential stem cells that exhibit myogenic, osteogenic, and adipogenic differentiation. *Differentiation* **68**, 245–253 (2001).
12. Shefer, G., Wleklinski-Lee, M. & Yablonka-Reuveni, Z. Skeletal muscle satellite cells can spontaneously enter an alternative mesenchymal pathway. *J. Cell Sci.* **117**, 5393–5404 (2004).
13. Uezumi, A. *et al.* Functional heterogeneity of side population cells in skeletal muscle. *Biochem. Biophys. Res. Commun.* **341**, 864–873 (2006).
14. Young, H. E. *et al.* Human reserve pluripotent mesenchymal stem cells are present in the connective tissues of skeletal muscle and dermis derived from fetal, adult, and geriatric donors. *Anat. Rec.* **264**, 51–62 (2001).
15. da Silva Meirelles, L., Chagastelles, P. C. & Nardi, N. B. Mesenchymal stem cells reside in virtually all post-natal organs and tissues. *J. Cell Sci.* **119**, 2204–2213 (2006).
16. Fukada, S. *et al.* Purification and cell-surface marker characterization of quiescent satellite cells from murine skeletal muscle by a novel monoclonal antibody. *Exp. Cell Res.* **296**, 245–255 (2004).
17. Orr-Urtreger, A., Bedford, M. T., Do, M. S., Eisenbach, L. & Lonai, P. Developmental expression of the α receptor for platelet-derived growth factor, which is deleted in the embryonic lethal Patch mutation. *Development* **115**, 289–303 (1992).
18. Shinbrot, E., Peters, K. G. & Williams, L. T. Expression of the platelet-derived growth factor β receptor during organogenesis and tissue differentiation in the mouse embryo. *Dev. Dyn.* **199**, 169–175 (1994).
19. De Palma, M. *et al.* Tie2 identifies a hematopoietic lineage of proangiogenic monocytes required for tumor vessel formation and a mesenchymal population of pericyte progenitors. *Cancer Cell* **8**, 211–226 (2005).
20. Farrington-Rock, C. *et al.* Chondrogenic and adipogenic potential of microvascular pericytes. *Circulation* **110**, 2226–2232 (2004).
21. Arsic, N. *et al.* Vascular endothelial growth factor stimulates skeletal muscle regeneration *in vivo*. *Mol. Ther.* **10**, 844–854 (2004).
22. Hawke, T. J. & Garry, D. J. Myogenic satellite cells: physiology to molecular biology. *J. Appl. Physiol.* **91**, 534–551 (2001).
23. Andrae, J., Gallini, R. & Betsholtz, C. Role of platelet-derived growth factors in physiology and medicine. *Genes Dev.* **22**, 1276–1312 (2008).
24. Orr-Urtreger, A. & Lonai, P. Platelet-derived growth factor-A and its receptor are expressed in separate, but adjacent cell layers of the mouse embryo. *Development* **115**, 1045–1058 (1992).
25. Darabi, R. *et al.* Functional skeletal muscle regeneration from differentiating embryonic stem cells. *Nature Med.* **14**, 134–143 (2008).
26. Takashima, Y. *et al.* Neuroepithelial cells supply an initial transient wave of MSC differentiation. *Cell* **129**, 1377–1388 (2007).
27. Morikawa, S. *et al.* Development of mesenchymal stem cells partially originate from the neural crest. *Biochem. Biophys. Res. Commun.* **379**, 1114–1119 (2009).
28. Morikawa, S. *et al.* Prospective identification, isolation, and systemic transplantation of multipotent mesenchymal stem cells in murine bone marrow. *J. Exp. Med.* **206**, 2483–2496 (2009).
29. Ball, S. G., Shuttleworth, C. A. & Kielty, C. M. Platelet-derived growth factor receptor-is a key determinant of smooth muscle α-actin filaments in bone marrow-derived mesenchymal stem cells. *Int. J. Biochem. Cell Biol.* **39**, 379–391 (2007).
30. Rodeheffer, M. S., Birsoy, K. & Friedman, J. M. Identification of white adipocyte progenitor cells *in vivo*. *Cell* **135**, 240–249 (2008).
31. Fukada, S. *et al.* CD90-positive cells, an additional cell population, produce laminin α2 upon transplantation to dy(3k)/dy(3k) mice. *Exp. Cell Res.* **314**, 193–203 (2008).
32. Aguiari, P. *et al.* High glucose induces adipogenic differentiation of muscle-derived stem cells. *Proc. Natl Acad. Sci. USA* **105**, 1226–1231 (2008).

METHODS

Animals. All procedures using experimental animals were approved by the Institutional Animal Care and Use Committee at Fujita Health University. C57BL/6 mice at 8 to 12 weeks old were purchased from SLC. GFP Tg mice (provided by M. Okabe, Osaka University, Japan) were maintained in our animal facility. Bone marrow transplantation was performed as described previously[31]. Mice were analysed 5 months after transplantation.

Cell preparation and FACS. Uninjured hind limb muscles or injured tibialis anterior muscles were excised and transferred into PBS. Nerves, blood vessels, tendons and fat tissues were carefully removed under a dissection microscope. Trimmed muscles were minced and digested with 0.2% type II collagenase (Worthington) for 45 min at 37 °C. Digested muscles were passed through an 18-gauge needle several times and further digested for 15 min at 37 °C. Muscle slurries were filtered through a 100 μm cell strainer (BD Biosciences) and through a 40 μm cell strainer (BD Biosciences). Erythrocytes were eliminated by treating the cells with Tris-buffered 0.8% NH_4Cl. Cells were resuspended in washing buffer consisting of PBS with 2.5% FBS, and stained with antibodies for 30 min at 4 °C. Secondary staining was then performed for 30 min at 4 °C in the dark. Antibodies and secondary reagents used for cell staining are listed in Supplementary Information, Table S1. Stained cells were analysed by FACSCalibur or FACSVantage SE (BD Biosciences). Cell sorting was performed on a FACSVantage SE. Debris and dead cells were excluded by forward scatter, side scatter and PI gating.

Cell culture. Freshly sorted cells were cultured on Matrigel-coated (BD Biosciences) eight-well chamber slides (Nalge Nunc) in growth medium (GM) consisting of DMEM supplemented with 20% FBS, 1% penicillin-streptomycin and 2.5 ng ml^{-1} bFGF (Invitrogen) for 4 days. 3T3-L1 cells were cultured in DMEM supplemented with 10% FBS and 1% penicillin-streptomycin. Ten thousands cells were plated per well. For adipogenic differentiation, cells were exposed for 3 days to adipogenic induction medium consisting of DMEM with 10% FBS, 0.5 mM IBMX (Sigma), 0.25 μM dexamethasone (Sigma) and 10 μg ml^{-1} insulin (Sigma), followed by adipogenic maintenance medium, consisting of DMEM with 10% FBS and 10 μg ml^{-1} insulin, for 3 days. For osteogenic differentiation, cells were treated for 4 days with osteogenic medium, which comprised 5% horse serum (HS) in DMEM supplemented with 500 ng ml^{-1} BMP7 (R & D Systems). For differentiation to the smooth muscle lineage, cells were treated for 4 days with 5 ng ml^{-1} TGF-β1 (R & D Systems) in DMED supplemented with 5% HS. For co-culture, 5×10^3 $CD31^-CD45^-SM/C\text{-}2.6^+$ cells sorted from wild-type mice and 1×10^4 $CD31^-CD45^-PDGFR\alpha^+$ cells sorted from GFP Tg mice were plated per well, and cultured in GM for 4 days followed by adipogenic treatment. For conditioned culture, $CD31^-CD45^-SM/C\text{-}2.6^+$ cells were cultured in GM for 4 days and were then treated with adipogenic induction medium for 1 day. The supernatant was collected and used as the satellite cell-conditioned medium. Cell culture inserts with 1.0-μm pore and 24-well culture plates (BD Biosciences) were used for transwell co-culture. Inserts and plates were coated with Matrigel. Freshly isolated 1×10^4 $CD31^-CD45^-SM/C\text{-}2.6^+$ cells were plated in the bottom of the plate, while 9×10^3 $CD31^-CD45^-PDGFR\alpha^+$ cells were plated in the upper insert. Transwell co-culture was maintained in GM for 4 days followed by adipogenic treatment.

Clonal assay. Freshly isolated $CD31^-CD45^-SM/C\text{-}2.6^-PDGFR\alpha^+$ cells were seeded onto a Matrigel-coated 96-well plate at a density of 0.8 cells per well and incubated for 8 days in GM at 37 °C in 5% CO_2 and 3% O_2. After 8 days of culture, colonies were treated with adipogenic induction medium (Adipo IM) for 3 days followed by treatment with adipogenic maintainence medium (Adipo MM) for 3 days at 37 °C in 5% CO_2 and 20% O_2.

RNA extraction and RT-PCR. Total RNA was extracted from 3×10^4 freshly sorted cells or cultured cells by using a RNeasy Micro Kit (Qiagen) and then reverse transcribed into cDNA using the QuantiTect Reverse Transcription Kit (Qiagen). The PCR reactions were performed with 0.5 μl cDNA product under the following cycling conditions: 94 °C for 3 min followed by 30 cycles of amplification (94 °C for 15 s, 60 °C for 30 s and 72 °C for 30 s) and a final incubation at 72 °C for 5 min. Real-time quantitative PCR was performed on a Thermal Cycler Dice Real Time System (Takara) with SYBR Premix Ex Taq (Takara) under the following cycling conditions: 95 °C for 10 s followed by 40 cycles of amplification (95 °C for 5 s, 60 °C for 15 s and 72 °C for 10 s) and dissociation curve analysis. Specific primer sequences used for PCR are listed in Supplementary Information, Table S2.

Muscle injury model. To induce fatty degeneration in skeletal muscle, 100 μl of 50% v/v glycerol was injected into tibialis anterior muscle with a 29-gauge needle. To induce muscle regeneration, 100 μl CTX (10 μM in saline; Sigma) was injected into the tibialis anterior muscle.

Intramuscular transplantation. Each cell population to be transplanted was isolated from GFP Tg mice. Immediately after cell sorting, 3×10^4 cells in 30 μl PBS were transplanted into the tibialis anterior muscles of wild-type mice that had been injected with glycerol or CTX. Two weeks after injury, tibialis anterior muscles were excised and fixed in 4% paraformaldehyde (PFA) for 30 min, immersed sequentially in 10% sucrose in PBS and 20% sucrose in PBS, and frozen in isopentane cooled with liquid nitrogen.

EdU administration. EdU (Invitrogen) was dissolved in PBS at 1 mg ml^{-1} and injected intraperitoneally at 0.1 mg per 20 g bodyweight, at the time points indicated.

Cytochemistry, histochemistry and microscopy. For staining cells immediately after isolation, FACS-sorted cells were collected by Cytospin3 (ThermoShandon). Cultured or cytospin-collected cells were fixed with 4% PFA for 5 min. Freshly frozen muscle tissues or frozen muscle tissues pre-fixed with PFA were sectioned (7-μm thick) using a cryostat. Fresh frozen sections were fixed with 4% PFA for 5 min. For Dlk1 and eMyHC staining, fresh frozen sections were fixed with acetone and methanol for 5 min at −20 °C, respectively. Specimens were blocked with protein-block serum-free reagent (DAKO) for 15 min, and incubated with primary antibodies at 4 °C overnight, followed by secondary staining. The M.O.M. kit (Vector) was used when mouse primary antibody was used to stain muscle sections. Antibodies used in this study are listed in Supplementary Information, Table S1. For EdU detection, the click chemical reaction was performed after primary and secondary staining according to the manufacture's instructions using the Click-iT EdU imaging kit (Invitrogen). Specimens were counterstained with DAPI (Invitrogen) and mounted with SlowFade Gold antifade reagent (Invitrogen). To stain lipids, cells and tissues were fixed in 10% formalin, rinsed in water and then 60% isopropanol, stained with oil red O in 60% isopropanol, and rinsed in water. Alkaline Phosphatase activity was determined using Sigma kit #85 in accordance with the manufacturer's instructions. In some cases, muscle sections were subjected to hematoxylin-eosin (HE) staining. For sequential immunohistochemistry, oil red O staining, and HE staining, immunofluorescence staining was performed first and immunofluorescent images were captured. Then slides were immersed in PBS to remove the mounted coverslip and subjected to oil red O staining. Oil red O images of corresponding fields were captured. Slides were immersed in PBS again to remove the coverslip and finally subjected to HE staining. Images of HE staining of corresponding fields were captured. In immunofluorescent and oil red O staining, SlowFade Gold antifade reagent was used as mounting medium. This mounting medium does not cure, therefore coverslip can be removed by immersing the slides in PBS. Stained cells and tissues were photographed using a fluorescence microscope BX51 (Olympus) equipped with a DP70 CCD camera (Olympus) or an inverted fluorescence microscope DMI4000B (Leica) equipped with a DFC350FX CCD camera (Leica). Confocal images of muscle sections were taken using the confocal laser scanning microscope system LSM510 (Carl Zeiss). See Supplementary Information, Table S1, for primary antibody dilutions.

Quantitative analysis. To measure the extent of differentiation of cultured cells, five to seven randomly selected fields were photographed per well. Images were collected and pooled from at least three independent experiments. The percentage of positive cells was determined by dividing the number of marker$^+$ cells by the number of $DAPI^+$ nuclei using Win ROOF software (Mitani Corp.) To assess the efficiency of transplantation, 7-μm thick transverse sections were obtained at 100-μm intervals throughout the muscle and were stained. The maximal number of GFP^+ myofibres and GFP^+ adipocytes were recorded. The numbers of $eMyHC^+EdU^+$ myofibres, myogenin$^+$ cells and $Pax7^+EdU^+$ cells were counted in representative transverse sections from the mid-belly of the muscles. The area occupied by regenerated myofibres, the area occupied by perilipin$^+$ adipocytes and the total area of tibialis anterior muscle were measured in representative transverse sections from the mid-belly of the muscles by using Win ROOF software. Data are represented as mean ± s.d.

Statistical analysis. Statistical significance was assessed by the Student's *t*-test. For comparisons of more than two groups, one-way analysis of variance (ANOVA) followed by Scheffe's test was used. *n* values for each experiment are indicated. A probability of less than 1% ($P < 0.01$) was considered statistically significant.

JPSA
Japan Poultry Science Association

http://www.jstage.jst.go.jp/browse/jpsa
doi:10.2141/jpsa.46.95

Expression Pattern of *WWP1* in Muscular Dystrophic and Normal Chickens

Hirokazu Matsumoto[1], Hideaki Maruse[1], Shinji Sasazaki[1], Akira Fujiwara[2], Shin'ichi Takeda[3], Nobutsune Ichihara[4,5], Tateki Kikuchi[3], Fumio Mukai[1] and Hideyuki Mannen[1]

[1] Laboratory of Animal Breeding and Genetics, Graduate School of Agricultural Science, Kobe University, Kobe 657-8501, Japan
[2] Laboratory Animal Research Station, Nippon Institute for Biological Science, Kobuchisawa 408-0041, Japan
[3] Department of Molecular Therapy and of [4] Animal Models for Human Disease, National Institute of Neuroscience, NCNP, Kodaira, Tokyo 182-8502, Japan
[5] Department of Anatomy I, School of veterinary medicine, Azabu University, Fuchinobe, Sagamihara, Kanagawa 229-8501, Japan

The WW domain containing E3 ubiquitin protein ligase 1 (WWP1) is classified into one of ubiquitin ligases which play an important role in ubiquitin-proteasome pathway. Previously, we identified the *WWP1* gene as a candidate gene of chicken muscular dystrophy by linkage analysis and sequence comparison. However, the mechanism causing pathological changes and underlaying gene function remains elucidated. In the present study, we analyzed the *WWP1* gene expression in various muscles and tissues of normal chickens, and compared with those from muscular dystrophic chickens. Two mRNA isoforms were detected in all tissues examined and revealed almost equal expression level. The *WWP1* expression of dystrophic chickens was decreased in almost all skeletal muscles including unaffected muscles. These data indicate that there might not be a causal relationship between the alteration of *WWP1* expression level and the severity of muscular dystrophy.

Key words: chicken, expression analysis, fast twitch muscle fiber, muscular dystrophy, WWP1

J. Poult. Sci., 46: 95-99, 2009

Introduction

The WW domain containing E3 ubiquitin protein ligase 1 (*WWP1*) is classified into an ubiquitin ligase (E3) which plays an important role in ubiquitin-proteasome pathway (UPP) to degrade unneeded or damaged proteins (Scheffner and Staub, 2007). E3 recognizes and catalyzes ubiquitin (Ub) conjugation to specific protein substrates (Liu, 2004). Comparative genome analysis reveals few genes encoding E1, tens of E2 encoding genes and hundreds of E3 encoding genes (Semple *et al.*, 2003).

The *WWP1* gene is classified into HECT (homologous to the E6-AP carboxyl terminus)-type E3 which possesses one C2 domain, multiple WW domains and one HECT domain (Pirozzi *et al.*, 1997; Flasza *et al.*, 2002). The C 2 domain binds to the cellular membranes in a Ca^{2+}-dependent manner (Plant *et al.*, 1997) and mediates interactions with other proteins (Plant *et al.*, 2000; von Poser *et al.*, 2000; Augustine, 2001). The WW domain has two conserved tryptophan residues and binds proline-rich region (Sudol *et al.*, 1985). HECT domain, similar to E2s structurally, has a cysteine residue as an active center that transfers the activated Ub from E2 onto first itself, and then onto its substrates (Jackson *et al.*, 2000).

The muscular dystrophies are the group of inherited diseases with progressive weakness and degeneration of skeletal muscle (Partridge, 1991). It is well known that abnormalities of muscle proteins linking sarcolemma and basal lamina lead to cause muscular dystrophies (Lisi and Cohn, 2007), but there are a number of muscular dystrophies and related diseases of which causes are still unknown. We identified *WWP1* gene as a candidate responsible for the chicken muscular dystrophy by the linkage analysis (Matsumoto *et al.*, 2007) and the sequence comparison between normal and dystrophic chickens (Matsumoto *et al.*, 2008). The R441Q missense mutation was found in *WWP1* gene to cause the phenotype of muscular dystrophy.

The WWP1s of human (Flasza *et al.*, 2002; Komuro *et al.*, 2004), mouse (Dallas *et al.*, 2006) and *C. elegans* (Huang *et al.*, 2000) were intensively studied and known

Received: October 10, 2008, Accepted: December 24, 2008
Correspondence: Dr. H. Mannen, Graduate School of Agricultural Science, Kobe University, Kobe 657-8501, Japan.
(E-mail: mannen@kobe-u.ac.jp)

that the *WWP1* gene is expressed ubiquitously, but strongly in liver, bone marrow, testis and skeletal muscles (Flasza *et al.*, 2002; Komuro *et al.*, 2004). In chicken, however, the *WWP1* expression has not been studied. The expression analysis of *WWP1* gene is important since it was reported that altered expression of known responsible gene could lead dystrophic phenotype (Smythe and Rando, 2006).

In this study, we analyzed the mRNA expression of *WWP1* in various skeletal muscles and other tissues of normal and dystrophic chickens by using Northern blotting and reverse transcription (RT)-PCR analysis to know the differences in the general expression pattern between them.

Materials and Methods

Chickens

A two-month-old dystrophic chicken (New Hampshire: NH-413) and an age-matched normal chicken (White Leghorn: WL-F) were used in this study. The New Hampshire (NH-413) strain is a homozygous dystrophic line introduced from University of California, Davis to Japan in 1976 (Kondo *et al.*, 1982). The disease in this strain is transmitted co-dominantly by a single gene, but the phenotype is modified by other background genes (Kikuchi *et al.*, 1981, 1987; Wilson *et al.*, 1979). The White Leghorn (WL-F) strain was established in 1970s, and maintained as closed colony in the Nippon Institute of Biological Science in Yamanashi, Japan. This study was carried out according to the guidelines of Animal Experimentation of Kobe University.

Expression analysis

For Northern blotting, mRNAs were isolated from *M. pectoralis superficialis* (PS), *M. tensor fascia lata* (TFL), *M. biceps femoris* (BF), *M. triceps surae* (TS), *M. peroneus longus* (PL), heart (H), brain (B), liver (L), kidney (K) and whole embryo (E) with PolyATtract mRNA Isolation kit (Promega, Madison, WI, USA). The 2μg of mRNAs, which were measured with NanoDrop ND-1000 spectrophotometer (NanoDrop Technologies, Wilmington, DE, USA), were resolved by 1.2% agarose gel electrophoresis in the presence of formaldehyde and blotted on to Hybond-N+membrane (GE Healthcare Bio-Sciences AB, Uppsala, Sweden). The mRNAs were visualized using digoxigenin (DIG) reagents, and kits for non-radioactive nucleic acid labeling and detection system (Roche Diagnostics, Basel, Switzerland) according to the procedure specified by the manufacturer excepting that the washing was done with 4×SCC 0.1% SDS at room temperature for 10 min, 4×SCC 0.1% SDS at 40°C for 8 min and then 2×SCC 0.1% SDS at 40°C for 8 min twice. The DIG-labeled DNA probes were prepared by PCR using DIG-dUTP using pectorals cDNA sample of a WL-F strain female as a template. The primers applied in this procedure were 5′-tccctcataaatgttgaaagcagaca-3′ (WWP1p-F), 5′-gtaataacccaaggtaatatgtaaac-3′ (WWP1 p-R) (NM_001012554), 5′-ccgtgtgccaacccccaatgt ctctg-3′ (GAPDHp-F) and 5′ -cagtttctatcagcctctcccacctc- 3′ (GAPDHp-R) (NM_204305). The PCR was done for 35 cycles at 94°C for 30 sec, 55°C for 30 sec, 72°C for 30 sec (*WWP1*) and for 35 cycles at 94°C for 30 sec, 63°C for 30 sec, 72°C for 30 sec (*GAPDH*) using TaKaRa Ex Taq® Hot Start Version (Takara Bio Inc., Tokyo, Japan). Quantitative analysis was performed with Scion Image (Scion Corporation, Frederick, MD, USA).

In order to analyze mRNA expression of *WWP1* gene in the PS, *M. anterior latissimus dorsi* (ALD) and H, RT-PCR method was applied. The concentration of cDNA derived from these muscles was calculated by NanoDrop ND-1000 (NanoDrop Technologies) and commeasurable cDNAs were used as template. The primers applied were 5′-attaggaagagccactgtagact-3′ (WWP1r-F) and 5′-tctgttgattgaggttctgctgt-3′ (WWP1r-R) (NM_001012554). The PCR was done for 35 and 40 cycles at 94°C for 30 sec, 56°C for 30 sec, 72°C for 30 sec using TaKaRa Ex Taq® Hot Start Version (Takara Bio Inc.).

Histology

The PS, ALD and H were snap-frozen in liquid nitrogen-cooled isopentane and sectioned in a cryostat (Leica Microsystems Japan, Tokyo, Japan). The histopathology was made by hematoxylin-eosin staining (HE) method (Kikuchi *et al.*, 1981).

Results

The mRNA expression of *WWP1* gene was detected by Northern blotting in various muscles and other tissues of normal and muscular dystrophic chickens (Fig. 1). Two bands were detected in all tissues examined, and revealed almost equally expression level in any muscles and tissues observed.

In the PS, BF, TS, PL, B and K, *WWP1* gene was strongly expressed in normal than in dystrophic chickens (Fig. 1). *GAPDH* was used as an internal control of *WWP 1* expression analysis. In TFL, L and E, similar *WWP1* expression level was observed between two phenotypes (Fig. 1).

RT-PCR analysis indicated that *WWP1* gene was expressed in slow tonic ALD, not only in PS and H of both phenotypes (Fig. 2A). Figure 2B shows histopathological changes in PS, ALD and H of normal and dystrophic chickens. The pathological findings in dystrophic PS were characterized by the degenerating fibers with many vacuoles in cytoplasm, the fatty infiltration into connective tissue, and the proliferation of nuclei within muscle fibers with large variation in sizes. However, no such lesions were observed in ALD and H from age-matched dystrophic chickens (Fig. 2B).

Discussion

Northern blotting with *WWP1* specific probe detected two bands in all tissues and muscles examined (Fig. 1). Northern blot analysis of *WWP1* expression in human tissues also exhibited two bands (Mosser *et al.*, 1998), and RT-PCR analysis showed that human *WWP1* gene had at

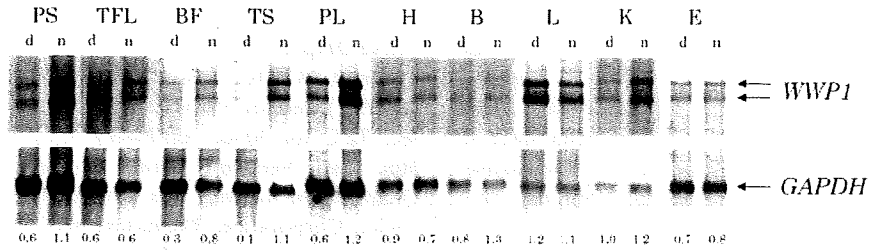

Fig. 1. **Expression of chicken *WWP1* in various tissues.**
A *WWP1* cDNA probe was used to detect *WWP1* mRNA transcripts by Northern blotting using blots containing 2μg of mRNAs from chicken muscles or various other tissues. *M. pectoralis superficialis* (PS), *M. tensor fascia lata* (TFL), *M. biceps femoris* (BF), *M. triceps surae* (TS), *M. peroneus longus* (PL), heart (H), brain (B), liver (L), kidney (K) and embryo (E) were analyzed. A doublet band is detected at variable levels in all tissues. "d" indicates mRNAs from dystrophic chickens. "n" indicates mRNAs from normal chickens. The numbers below the *GAPDH* bands represent the relative ratios of *WWP1/GAPDH*.

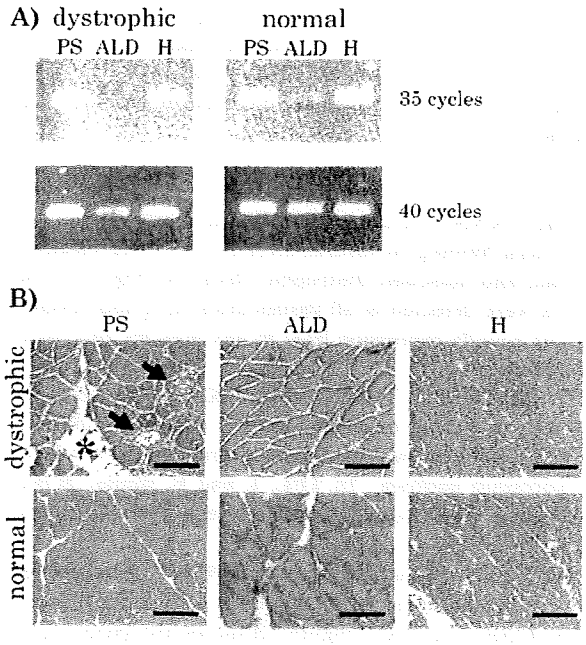

Fig. 2. **RT-PCR detection of *WWP1* gene and histological analysis for three representative muscle types.**
M. pectoralis superficialis (PS), *M. anterior latissimus dorsi* (ALD) and heart (H) expressed *WWP1* less in muscular dystrophic chicken, but only dystrophic PS was severely harmed. A) Expression of *WWP1* in PS, ALD and H was analyzed by RT-PCR method. PCR was performed for 35 or 40 cycles. B) The PS, ALD and H of dystrophic (NH-413) and normal (WL-F) chickens were analyzed with HE staining. Vacuoles (arrows) and fatty infiltration (asterisk) are observed in PS of dystrophic chickens. It is also remarkable that, in dystrophic PS, many muscle fibers have many nuclei in cytoplasm and vary widely in size. These pathological features are not observed in ALD and H of dystrophic chicken. Scale bar=120μm.

least six mRNA isoforms synthesized through the alternative splicing, two of which were strongly expressed and commonly observed in various tissues (Flasza *et al.*, 2002). The mRNA doublet bands of chicken *WWP1* by Northern blot analysis might be equivalent to two bands of human tissues, while a single band was observed by RT-PCR analysis in chicken (Fig. 2A), suggesting that the amplified region does not include alternative spliced site. Flasza *et al.* (2002) also mentioned that the relative ratio of these isoforms from human *WWP1* varied in a tissue-specific manner, but the doublet bands of chicken *WWP1* were expressed almost equally in all tissues examined.

The *WWP1* gene expression in *M. pectoralis superficialis* (PS) of dystrophic chicken was less than that of normal chicken (Fig. 1). The PS of chicken is a fast twitch muscle composed of two types of fast twitch fibers (aW and bW). TFL, BF, TS and PL muscles from wing and leg are mixed muscles co-existing fast twitch (aW and bW) with slow twitch fibers (bR) in a mosaic pattern (Ashmore and Doerr, 1971a), except that the ALD and *M. adductor magnus* are composed of slow tonic fibers (ST) innervated multiply (Ashmore *et al.*, 1978; Kikuchi *et al.*, 1986). In chicken muscular dystrophy, fast twitch fibers are initially and most severely affected, while slow twitch and slow tonic muscles persist relatively harmless throughout the life span (Ashmore and Doerr, 1971b; Barnard *et al.*, 1982). The *WWP1* expression in dystrophic BF, TS and PL showed a similar downward trend as observed in dystrophic PS (Fig. 1). These data indicate that there might not be a causal relationship between the alteration of *WWP1* expression level and the severity of muscular dystrophy, since not only affected muscles but unaffected ones exhibited the same pattern. Moreover, the alteration of *WWP1* expression level was observed in other unaffected tissues, such as B and K, which reinforces our hypothesis that the alteration of *WWP1* expression levels

does not link directly to the dystrophic phenotype (Fig. 1).

To assess the genetic influence of mutant *WWP1* upon chicken muscular dystrophy, we examined *WWP1* gene expression and histological changes in three distinct muscle types, PS as a fast twitch type, ALD as a slow tonic type, and H as a different type of muscle. RT-PCR was applied to this study since ALD was not enough quantity of mRNA for Northern blotting. The *WWP1* mRNA expression was confirmed in all muscles examined (Fig. 2 A).

Figure 2B shows HE stained sections of PS, ALD and H from normal and dystrophic chicken. The dystrophic PS was severely affected, while ALD and heart of dystrophic chicken remained relatively intact (Fig. 2B) as described in a previous study (Kikuchi *et al.*, 1981). The *WWP1* was expressed even in unaffected muscles and the downward alteration of *WWP1* expression was observed commonly in almost all dystrophic muscles examined (Figs. 1, 2). The observation suggests that the alteration of *WWP1* might not be the cause of the pathological change in chicken muscular dystrophy. Hence, the mutation identified previously (Matsumoto *et al.*, 2008) might play a crucial role in leading the onset of chicken muscular dystrophy. The detected mutation lay between WW domains, highly conserved region among tetrapods (Matsumoto *et al.*, 2008), which has been predicted as substrate binding region (Pirozzi *et al.*, 1997; Flasza *et al.*, 2002). This suggests that mutated *WWP1* could not recognize its substrates.

Many HECT-type E3s with WW domains including *WWP1* regulate membrane proteins (Chen and Matesic, 2007). Therefore, aberrant regulation of membrane protein may lead the onset of chicken muscular dystrophy. For example, *WWP1* could bind to β-dystroglycan, which is one of important muscle proteins consisting of membrane (Pirozzi *et al.*, 1997). Abnormal glycosylation of α-dystroglycan in chicken muscular dystrophy has been reported (Saito *et al.*, 2005). Furthermore, the fact that some E3s can recognize sugar chain (Yoshida *et al.*, 2002, 2003; Lederkremer and Gliskman, 2005) leads to the hypothesis that mutated *WWP1* might not be able to recognize the sugar chain of α-dystroglycan to regulate the glycosylated molecules, and that insufficiently glycosylated α-dystroglycan accumulates and causes the disease.

In the present study, we analyzed the mRNA expression of *WWP1* in various skeletal muscles and other tissues of normal and dystrophic chickens. The results suggest that *WWP1* expression level lowered in dystrophic phenotype is not directly related to the cause of disease in chicken muscular dystrophy, whereas mutated *WWP1* does not function normally to cause the onset of chicken muscular dystrophy.

Acknowledgments

This work was supported in part by Grant-in-Aid for Scientific Research (C), no. 19580338, and the Global COE Program "Global Center for Education and Research in Integrative Membrane Biology" (A-8) from the Ministry of Education, Science, Sports and Research on Nervous and Mental Disorders (16B-2, 19A-7) from the Japanese Ministry of Health, Labor and Welfare.

References

Ashmore CR and Doerr L. Comparative aspects of muscle fiber types in different species. Experimental Neurology, 31: 408–418. 1971a.

Ashmore CR and Doerr L. Postnatal development of fiber types in normal and dystrophic skeletal muscle of the chick. Experimental Neurology, 30: 431–446. 1971b.

Ashmore CR, Kikuchi T and Doerr L. Some observations on the innervation patterns of different fiber types of chick muscle. Experimental Neurology, 58: 272–284. 1978.

Augustine GJ. How does calcium trigger neurotransmitter release? Current Opinion in Neurobiology, 11: 320–326. 2001.

Barnard EA, Lyles JM, and Pizzey JA. Fibre types in chicken skeletal muscles and their changes in muscular dystrophy. The Journal of Physiology, 331: 333–354. 1982.

Chen C and Matesic LE. The Nedd4-like family of E3 ubiquitin ligases and cancer. Cancer Metastasis Reviews, 3–4: 587–604. 2007.

Dallas CJ, Marc NW, Mohamed O, Jochen GH, Melvin JG and Laurie HG. Regulation of Adult Bone Mass by the Zinc Finger Adapter Protein Schnurri-3. Science, 312: 1223–1227. 2006.

Flasza M, Gorman P, Roylance R, Canfield AE and Baron M. Alternative Splicing Determines the Domain Structure of WWP1, a Nedd4 Family Protein. Biochemical and Biophysical Research Communications, 290: 431–437. 2002.

Huang K, Johnson KD, Petcherski AG, Vandergon T, Mosser EA, Copeland NG, Jenkins NA, Kimble J and Bresnick EH. A HECT domain ubiquitin ligase closely related to the mammalian protein WWP1 is essential for Caenorhabditis elegans embryogenesis. Gene, 252: 137–145. 2000.

Jackson PK, Eldridge AG, Freed E, Furstenthal L, Hsu JY, Kaiser BK and Reimann JDR. The lore of the RINGs: substrate recognition and catalysis by ubiquitin ligases. Trends in Cell Biology, 10: 429–439. 2000.

Kikuchi T, Akiba T and Ashmore CR. Conversion of muscle fiber types in regenerating chicken muscles following cross-reinnervation. Acta Neuropathologica, 71: 197–206. 1986.

Kikuchi T, Ishiura S, Nonaka I and Ebashi S. Genetic heterozygous carriers in hereditary muscular dystrophy of chickens. Tohoku Journal of Agriculture Research, 32: 14–26. 1981.

Kikuchi T, Moriya H, Matuzani T, Katoh M and Takeda S. The development of laboratory animal science for the study of human muscular and nervous diseases in Japan. Congenital Anomalies, 27: 447–462. 1987.

Komuro A, Imamura T, Saitoh M, Yoshida Y, Yamori T, Miyazono K and Miyazawa K. Negative regulation of transforming growth factor-beta (TGF-beta) signaling by WW domain-containing protein 1 (WWP1). Oncogene, 23: 6914–6923. 2004.

Kondo K, Kikuchi T and Mizutani M. Breeding of the chicken as an animal model for muscular dystrophy. In: Muscular Dystrophy (Ebashi S ed.), pp. 19–24. Tokyo University

Press. Tokyo. 1982.
Lederkremer GZ and Glickman MH. A window of opportunity: timing protein degradation by trimming of sugars and ubiquitins. Trends in Biochemical Sciences, 30: 297-303. 2005.
Lisi MT and Cohn RD. Congenital muscular dystrophies: new aspects of an expanding group of disorders. Biochimica et Biophysica Acta, 1772: 159-172. 2007.
Liu YC. Ubiquitin ligases and the immune response. Annual Review of Immunology, 22: 81-127. 2004.
Matsumoto H, Maruse H, Yoshizawa K, Sasazaki S, Fujiwara A, Kikuchi T, Ichihara N, Mukai F and Mannen H. Pinpointing the candidate region for muscular dystrophy in chickens with an abnormal muscle gene. Animal Science Journal, 78: 476-483. 2007.
Matsumoto H, Maruse H, Inaba Y, Yoshizawa K, Sasazaki S, Fujiwara A, Nishibori M, Nakamura A, Takeda S, Ichihara N, Kikuchi T, Mukai F and Mannen H. The ubiquitin ligase gene (WWP1) is responsible for the chicken muscular dystrophy. FEBS Letters, 582: 2212-2218. 2008.
Mosser EA, Kasanov JD, Forsberg EC, Kay BK, Ney PA and Bresnick EH. Physical and functional interactions between the transactivation domain of the hematopoietic transcription factor NF-E2 and WW domains. Biochemistry, 37: 13686-13695. 1998.
Partridge T. Animal models of muscular dystrophy: what can they teach us? Neuropathology and Applied Neurobiology, 17: 353-363. 1991.
Pirozzi G, McConnell SJ, Uveges AJ, Carter JM, Sparksi AB, Kayi BK and Fowlkes DM. Identification of Novel Human WW Domain-containing Proteins by Cloning of Ligand Targets. The Journal of Biological Chemistry, 272: 14611-14616. 1997.
Plant PJ, Lafont F, Lecat S, Verkade P, Simons K and Rotin D. Apical membrane targeting of Nedd4 is mediated by an association of its C2 domain with annexin XIIIb. The Journal of Cell Biology, 149: 1473-1484. 2000.
Plant PJ, Yeger H, Staub O, Howard P and Rotin D. The C2 domain of the ubiquitin protein ligase Nedd4 mediates Ca^{2+}-dependent plasma membrane localization. The Journal of Biological Chemistry, 272: 32329-32336. 1997.
Saito F, Blank M, Schroder J, Manya H, Shimizu T, Campbell KP, Endo T, Mizutani M, Kroger S and Matsumura K. Aberrant glycosylation of a-dystroglycan causes defective binding of laminin in the muscle of chicken muscular dystrophy. FEBS Letters, 579: 2359-2363. 2005.
Scheffner M and Staub O. HECT E3s and human disease. BMC Biochemistry, 8 Suppl 1: S6. 2007.
Semple CA, RIKEN GER Group and GSL Members. The comparative proteomics of ubiquitination in mouse. Genome Research, 13: 1389-1394. 2003.
Smythe GM and Rando TA. Altered caveolin-3 expression disrupts PI (3) kinase signaling leading to death of cultured muscle cells. Experimental cell research, 312: 2816-2825. 2006.
Sudol M, Chen HI, Bougeret C, Einbond A and Bork P. Characterization of a novel protein-binding module: the WW domain. FEBS Letters, 369: 67-71. 1985.
von Poser C, Zhang JZ, Mineo C, Ding W, Ying Y, Sudhof TC and Anderson RG. Synaptotagmin regulation of coated pit assembly. The Journal of Biological Chemistry, 275: 30916-30924. 2000.
Wilson BW, Randall WR, Patterson GT and Entrikin RK. Major physiologic and histochemical characteristics of inherited dystrophy of the chicken. Annals of the New York Academy of Sciences, 317: 224-246. 1979.
Yoshida Y, Chiba T, Tokunaga F, Kawasaki H, Iwai K, Suzuki T, Ito Y, Matsuoka K, Yoshida M, Tanaka K and Tai T. E 3 ubiquitin ligase that recognizes sugar chains. Nature, 418: 438-442. 2002.
Yoshida Y, Tokunaga F, Chiba T, Iwai K, Tanaka K and Tai T. Fbs2 is a new member of the E3 ubiquitin ligase family that recognizes sugar chains. The Journal of Biological Chemistry, 278: 43877-43884. 2003.

ABSTRACT: Duchenne muscular dystrophy (DMD) is a devastating muscle disorder that is characterized by progressive muscle necrosis, fibrosis, and fatty infiltration. To examine the temporospatial pathological changes, a noninvasive evaluation method such as magnetic resonance imaging (MRI) is needed. The aim of this study was to precisely assess muscle necrosis and inflammation based on a sequence of T2-weighted imaging (T2WI), gadolinium-enhanced imaging, and selective fat suppression, chemical shift selective T2-weighted imaging (CHESS-T2WI), on a 3.0-Tesla MRI unit in 3-month-old and 7-year-old dogs with canine X-linked muscular dystrophy ($CXMD_J$), a suitable animal model for DMD. The results show that CHESS-T2WI was more sensitive and useful from the early to late stages of $CXMD_J$ than T2WI or contrast enhancement imaging in the evaluation of muscle necrosis, because these latter sequences can be influenced by fatty infiltration or interstitial connective tissues.

Muscle Nerve **40:** 815–826, 2009

EVALUATION OF DYSTROPHIC DOG PATHOLOGY BY FAT-SUPPRESSED T2-WEIGHTED IMAGING

MASANORI KOBAYASHI, DVM,[1,2] AKINORI NAKAMURA, MD, PhD,[1] DAISUKE HASEGAWA, DVM, PhD,[2] MICHIO FUJITA, DVM, PhD,[2] HIROMITSU ORIMA, DVM, PhD,[2] and SHIN'ICHI TAKEDA, MD, PhD[1]

[1] Department of Molecular Therapy, National Institute of Neuroscience, NCNP, 4-1-1 Ogawa-higashi, Kodaira, Tokyo 187-8502, Japan
[2] Department of Veterinary Radiology, Nippon Veterinary and Life Science University, Tokyo, Japan

Accepted 23 March 2009

Duchenne muscular dystrophy (DMD) is a severe X-linked muscle disease characterized by progressive skeletal muscle atrophy and weakness.[1] DMD is caused by mutations in the *dystrophin* gene, which encodes the cytoskeletal protein dystrophin.[2] A loss of dystrophin accompanied by a deficiency of dystrophin–glycoprotein complex (DGC) from the sarcolemma leads to progressive degeneration of striated muscle.[3,4] In dystrophic skeletal muscles, muscle fiber necrosis with inflammation is followed by muscle regeneration, but the muscle is finally replaced by fibrous or fatty tissue.[5,6] For this devastating disorder, various therapeutic approaches, such as gene therapy, stem cell–based cell therapy, or pharmaceutical agents have been proposed and explored using various DMD animal models.

The X-linked muscular dystrophy (*mdx*) mouse and Golden Retriever muscular dystrophy (GRMD) dog are the most commonly used DMD animal models.[7,8] *mdx* mice show extensive necrosis followed by regeneration, but their phenotypes are milder than those of DMD due to the absence of apparent fibrosis and fatty infiltration.[7,9,10] The phenotypes of striated muscle in the GRMD dog are clinically and pathologically more similar to that of DMD,[8,11,12] but it is very difficult to maintain this animal model due to the severe phenotype. We have therefore established a Beagle-based colony of canine X-linked muscular dystrophy in Japan ($CXMD_J$).[13] We have found that the clinical and pathological findings in $CXMD_J$ are similar to but milder than those in GRMD.[14,15]

A method of noninvasive temporospatial assessment is required to investigate muscle involvement and, especially, to evaluate therapeutic

Abbreviations: ANOVA, analysis of variance; CE, contrast enhancement ratio; CHESS, chemical shift selective; CT, computed tomography; $CXMD_J$, canine X-linked muscular dystrophy in Japan; DGC, dystrophin–glycoprotein complex; DMD, Duchenne muscular dystrophy; EDL, extensor digitorum longus; FDS, flexor digitorum superficialis; FITC, fluorescein isothiocyanate; GC, gastrocnemius; Gd-DTPA, gadolinium diethylenetriamine pentaacetic acid; GMRD, Golden Retriever muscular dystrophy; MRI, magnetic resonance imaging; PCr, phosphocreatine; Pi, inorganic phosphate; ROI, region of interest; SNR, signal-to-noise ratio; STIR, short-tau inversion recovery; SI, signal intensity; TC, tibialis cranialis

Key words: chemical shift selective fat-suppressed T2-weighted imaging; Duchenne muscular dystrophy; dystrophic dog; magnetic resonance imaging; myopathy

Correspondence to: S. Takeda; e-mail: takeda@ncnp.go.jp

Published online 7 August 2009 in Wiley InterScience (www.interscience.wiley.com). DOI 10.1002/mus.21384

interventions. Computed tomography (CT), which shows high temporal and spatial resolution, has been used to detect selective muscle involvement, such as atrophy or fatty tissue replacement, in patients suffering from DMD,[16,17] but it requires ionizing radiation and has limited sensitivity for soft tissues.[18] Magnetic resonance imaging (MRI) produces high-resolution images with good contrast among soft tissues,[19] and therefore it has been used to evaluate skeletal muscle involvement in DMD[20] and in *mdx* mice.[21] In the early stages of dystrophy, the T1 relaxation time is prolonged due to muscle degeneration and regeneration together with an increase in muscle water concentration, and it is decreased owing to fat infiltration in the advanced stage.[22] As the main magnetic field increases, however, the capacity to differentiate tissues on the basis of T1 relaxation time may decrease.[23] On the other hand, the T2 relaxation time is prolonged in necrotic as well as fatty and connective tissue[19]; therefore, it can hardly distinguish necrosis from fat replacement or fibrosis during the dystrophic process. To selectively detect necrotic changes, MR contrast agents, such as gadolinium diethylenetriamine pentaacetic acid (Gd-DTPA), have been used extensively,[24–26] but these agents may also enhance blood vessels and the interstitium,[27] and may cause severe adverse effects, such as anaphylaxis,[28,29] which are critical for DMD patients. Thus, a safer imaging protocol is needed to distinguish necrotic lesions from fatty degeneration or fibrosis in the dystrophic skeletal muscle of DMD and $CXMD_J$.

To discriminate necrosis from fatty infiltration, one of the fat suppression sequences may be useful. As a fat suppression sequence, short-tau inversion recovery (STIR) MR imaging was used to detect muscle edema in DMD.[6] However, STIR suppresses the signal from any tissue or fluid that has a short T1 relaxation time, and therefore it does not selectively suppress the fat signal.[30,31] In contrast, chemical shift selective (CHESS) imaging, another fat suppression sequence, is a technique that selectively saturates fat magnetization by applying a 90° pulse matching with the fat resonance frequency and therefore leads to a highly selective suppression of fat signals. Moreover, the signal-to-noise ratio (SNR) of CHESS is better than that of STIR at a higher magnetic field. The sequence of CHESS combined with T2-weighted imaging (CHESS-T2WI) has been used to diagnose disorders such as lipomatous tumor or temporomandibular arthrosis.[32–34] The method, however, has not been applied to evaluation of the dystrophic changes seen in DMD or the animal models to date.

We, therefore, examined dystrophic dog muscle by CHESS-T2WI to determine whether this sequence is more useful for finding necrosis and inflammatory change than the conventional sequences of T2WI or contrast imaging.

METHODS

Animals. We used three 3-month-old normal male dogs (II-2308MN, II/III-3911MN, and II-4202MN), three littermate $CXMD_J$ male dogs (II-2302MA, II/III-3903MA, and II-4204MA), one 7-year-old normal male dog (00-174MN), and two 7-year-old $CXMD_J$ male dogs (II-C04MA and II-C12MA). II-2308MN, II-4202MN, II-2302MA, and II-4204MA were produced by mating a second-generation (G2) carrier female[13] and G2 affected male. II/III-3911MN and II/III-3903MA were the offspring of a G2 carrier female and a third-generation (G3) affected male. We obtained II-C04MA and II-C12MA by mating first-generation (G1) carrier female dogs and pure-bred normal male Beagles. 00-174MN was a pure-bred normal Beagle. All dogs were part of the breeding colony at the General Animal Research Facility, National Institute of Neuroscience, National Center of Neurology and Psychiatry (Tokyo, Japan), or the Chugai Research Institute for Medical Science, Inc. (Nagano, Japan). Ages, body weights, and serum creatine kinase values at the time of MRI of each dog are shown in Table 1. This study was carried out according to the guidelines provided by the Ethics Committee for the Treatment of Middle-sized Laboratory Animals of the National Center of Neurology and Psychiatry (Approval Nos. 18-02, 19-02, and 20-02).

MR Scanning and Image Analysis. General anesthesia was induced by an intravenous injection of thiopental sodium (20 mg/kg) before MRI scanning and was maintained by inhalation of isoflurane (2.0–3.0%). We examined lower leg muscles of these dogs by superconducting 3.0-Tesla MRI (Magnetom Trio; Siemens Medical Solutions, Erlangen, Germany) with a human extremity coil 18 cm in diameter. The MRI pulse sequences used were T1-weighted imaging (T1WI), T2WI, chemical shift selective T1-weighted imaging (CHESS-T1WI), CHESS-T2WI, gadolinium-enhanced T1-weighted imaging (Gd-T1WI), chemical shift selective gadolinium-enhanced T1-weighted imaging (CHESS-

Table 1. Clinical profiles of normal and dystrophic male dogs used in this study.

	Age (mo)	BW (kg)	Serum CK (IU/L)
Normal dogs			
II-2308MN	3	6.8	197
II/III-3911MN	3	7.7	318
II-4202MN	3	5.8	274
00-174MN	87	13.7	83
CXMDJ dogs			
II-2302MA	3	7.2	30,200
II/III-3903MA	3	6.6	22,300
II-4204MA	3	6.0	28,800
II-C04MA	85	11.5	6500
II-C12MA	94	11.6	1602

Body weight (BW) and serum creatine kinase (CK) values were measured on the day of MRI examination.

Gd-T1WI), and multi-echo T2WI for calculation of T2 relaxation time. In contrast-enhanced images, we injected 0.2 ml/kg of the gadolinium-based MR contrast agent Gd-DTPA (Magnevist; Bayer Schering Pharma, Berlin, Germany) for each sequence. In 3-month-old dogs, we scanned the images for 26 minutes, about 5 minutes after the intravenous injection. On the other hand, we took the images for 13 minutes in 7-year-old dogs at 25 minutes after the injection in order to minimize the risk of anesthesia on the cardiac involvement seen in advanced $CXMD_J$.[15] CHESS was employed to assess necrotic and inflammatory changes more precisely. The acquisition parameters for T1WI, CHESS-T1WI, Gd-T1WI, and CHESS-Gd-T1WI were based on spin echo: repetition time (TR)/echo time (TE) = 500/7.4 ms; slice thickness = 4 mm; field of view = 18 × 18 cm; matrix = 256 × 256; and NEX = 3. The parameters for T2WI and CHESS-T2WI were chosen based on fast spin echo: TR/TE = 4000/85 ms; slice thickness = 4 mm; field of view = 18 × 18 cm; matrix = 256 × 256; turbo-factor = 9; and NEX = 3. The parameters for multi-echo T2WI were selected based on spin echo: TR = 2000; TE = 11.8–118.0 (10 echoes); slice thickness = 4 mm; field of view = 28 × 28 cm; matrix = 256 × 256; and NEX = 2. We were able to clearly distinguish each lower leg muscle by each sequence. Representative cross-sectional images and anatomical locations of lower leg muscles by CHESS-T1WI in a 7-year-old normal dog are shown in Figure 1.

For quantitative analysis of the images, the manufacturer's software (Syngo MR2004A; Siemens Medical Solutions, Erlangen, Germany) was used. Flow artifacts were slight, but regions of interest (ROIs) were selected to avoid flow artifacts and large vessels as follows: three circular ROIs were picked in both right tibialis cranialis (Rt. TC) and extensor digitorum longus (Rt. EDL) muscles of the 3-month-old dogs. ROIs were also selected in the Rt. TC of the 7-year-old dogs and a normal dog. Then, T2 relaxation time or signal intensities (SIs) of CHESS-T1WI, CHESS-Gd-T1WI, and CHESS-T2WI were measured in these ROIs. Signal-to-noise ratios (SNRs) of each ROI were calculated by the equation: $SNR = SI/SD_{air}$, where SD_{air} was the standard deviation (SD) of background noise.[35] The contrast enhancement (CE) ratio was calculated using the SNR of CHESS-T1WI ($SNR_{precontrast}$) and SNR of CHESS-Gd-T1WI ($SNR_{postcontrast}$) by the following equation: $CE = SNR_{postcontrast}/SNR_{precontrast}$. We used the means of the quantitative values at three points of ROIs for statistical analysis.

Statistical Analysis. The T2 relaxation time, CE ratio, and SNR of CHESS-T2WI were evaluated using a one-way analysis of variance (ANOVA) to determine differences among the groups. When a significant difference was found with one-way ANOVA, intergroup comparisons were undertaken using Fisher's protected least significant difference test. All values are expressed as mean ± SE, and statistical significance was recognized at $P < 0.05$.

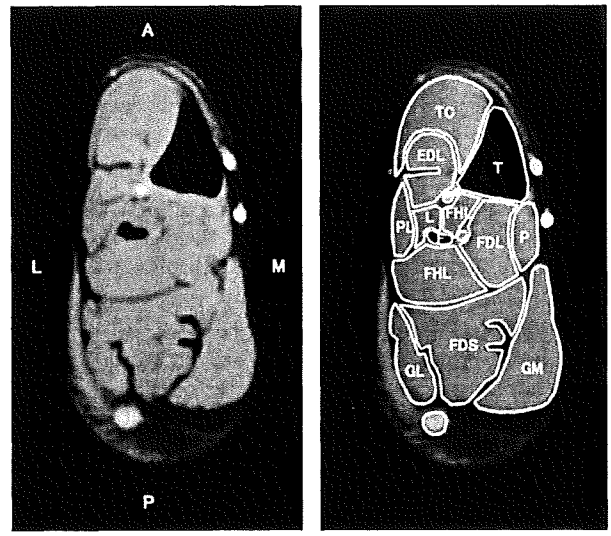

FIGURE 1. Cross-sectional images and anatomical orientation of right lower leg muscles of a 7-year-old normal dog in CHESS-T1WI. A 7-year-old normal dog (00-174MN) was used for this study. T, tibia; F, fibula; TC, tibialis cranialis; EDL, extensor digitorum longus; FHL, flexor hallucis longus; FDL, flexor digitorum longus; FDS, flexor digitorum superficialis; GM, gastrocnemius medialis; GL, gastrocnemius lateralis. A, anterior; P, posterior; L, lateral side; M, medial side.

Histopathology. We performed muscle biopsies of the right TC and right EDL on a 3-month-old normal dog (II-2308MN) and a $CXMD_J$ dog (II-2302MA), and right TC on a 7-year-old normal dog (00-174MN) and a $CXMD_J$ dog (II-C04MA) after MRI scanning. The muscle samples were snap-frozen in liquid nitrogen cooled by isopentane. Hematoxylin and eosin (H&E) staining was performed on serial 10-μm transverse cryostat sections. Anti-IgG immunofluorescence staining was performed on 6-μm serial cryostat sections incubated with fluorescein isothiocyanate (FITC)-conjugated polyclonal sheep anti-canine IgG (1:200; AbD Serotec, Oxford, UK) overnight. To examine fatty infiltration in the muscle, 6-μm serial frozen sections from normal and $CXMD_J$ dogs at 7 years of age were stained with oil red O.

RESULTS

MRI Findings of Lower Leg Muscles in 3-Month-Old Normal Dogs. First, we acquired muscle images of three 3-month-old normal dogs by T1WI, T2WI, CHESS-T1WI, CHESS-T2WI, Gd-T1WI, and CHESS-Gd-T1WI. Representative cross-sectional images of II-2308MN are shown in Figure 2A. In normal dogs, the lower leg muscles showed a homogeneous signal intensity in these sequences, but the muscles that contain mainly slow-twitch fibers, such as the gastrocnemius (GC) and flexor digitorum superficialis (FDS) (Fig. 2A, e and i), showed slight hyperintensity on T2WI and CHESS-T2WI when compared with muscles that contain mainly fast-twitch fibers such as TC and EDL (Fig. 2A, e and i). These findings were consistent with the previous T2 relaxation time study of rabbit muscles.[36] Gd-T1WI (data not shown) or CHESS-Gd-T1WI (Fig. 2A, g) showed homogeneous and slight enhancement when compared with T1WI (Fig. 2A, a) or CHESS-T1WI (Fig. 2A, c), respectively, in all normal dogs.

MRI Findings of Lower Leg Muscles in 3-Month-Old Dystrophic Dogs. Next, we tried to detect muscle involvement in three 3-month-old $CXMD_J$ dogs. Clinically, the dogs showed mild to moderate muscle atrophy and gait or mobility disturbance. These clinical findings are compatible with our previous study of $CXMD_J$dogs.[14] Representative cross-sectional images of II-2302MA are shown in Figure 2A.

All lower leg muscles of the three $CXMD_J$ showed no change on T1WI and CHESS-T1WI (Fig. 2A, b and d), but almost all lower leg muscles, especially EDL and GC, revealed remarkable hyperintensity on T2WI when compared with the images of normal dogs. We should note that the hyperintensity on TC was rather slight compared with that of the other lower leg muscles (Fig. 2A, f). We found that contrast agent uptake by Gd-T1WI (data not shown) or CHESS-Gd-T1WI (Fig. 2A, h) was increased in the areas where hyperintensity was recorded by T2WI. These findings suggest the necrotic and/or inflammatory changes that were shown in a previous study of *mdx* mice.[21] Hyperintensity was also clearly indicated by CHESS-T2WI in these regions, where hyperintensity on T2WI and contrast agent uptake in Gd-T1WI or CHESS-Gd-T1WI were noted (Fig. 2A, j).

Comparison of MR Signal Intensities of 3-Month-Old Normal and Dystrophic Dogs. To quantitatively evaluate MRI findings of three normal and three $CXMD_J$ dogs, we measured T2 relaxation time, CE based on comparison between SNR of CHESS-T1WI and CHESS-Gd-T1WI, and SNR of CHESS-T2WI. In TC, the T2 relaxation time of $CXMD_J$ dogs was significantly prolonged (49.8 $\pm$ 2.3 ms) when compared with that of normal dogs (39.9 $\pm$ 1.2 ms) ($P = 0.0004$). Moreover, T2 relaxation time of EDL was significantly prolonged in $CXMD_J$ (58.6 $\pm$ 3.1 ms) when compared with not only that in normal dogs (40.0 $\pm$ 0.5 ms) but also that of TC in $CXMD_J$ dogs ($P < 0.0001$ and $P = 0.0008$, respectively) (Fig. 2B, a).

Similarly, the effect of contrast enhancement in TC and EDL of $CXMD_J$ (1.659 $\pm$ 0.077 and 1.936 $\pm$ 0.127-fold) was significantly increased in comparison with that of normal dogs (1.511 $\pm$ 0.009 and 1.528 $\pm$ 0.015 fold) ($P = 0.0413$ and $P = 0.0002$, respectively), but the effect in TC of $CXMD_J$ was more prominent in EDL of $CXMD_J$ ($P = 0.0019$) (Fig. 2B, b).

In TC, the SNR of CHESS-T2WI was significantly increased in $CXMD_J$ (102.3 $\pm$ 12.1) when compared with that of normal dogs (70.0 $\pm$ 3.6) ($P = 0.0019$). Moreover, the SNR of CHESS-T2WI was significantly increased in EDL of $CXMD_J$ (146.0 $\pm$ 11.7) when compared with not only that of normal dogs (69.2 $\pm$ 2.9) but also that in TC of $CXMD_J$ dogs ($P < 0.0001$ and $P = 0.0003$, respectively), indicating EDL was more affected than TC in the early stage of $CXMD_J$ (Fig. 2B, c).

Histopathological Findings in Lower Leg Muscles of 3-month-old Normal and Dystrophic Dogs. To determine the relationship between MRI findings and

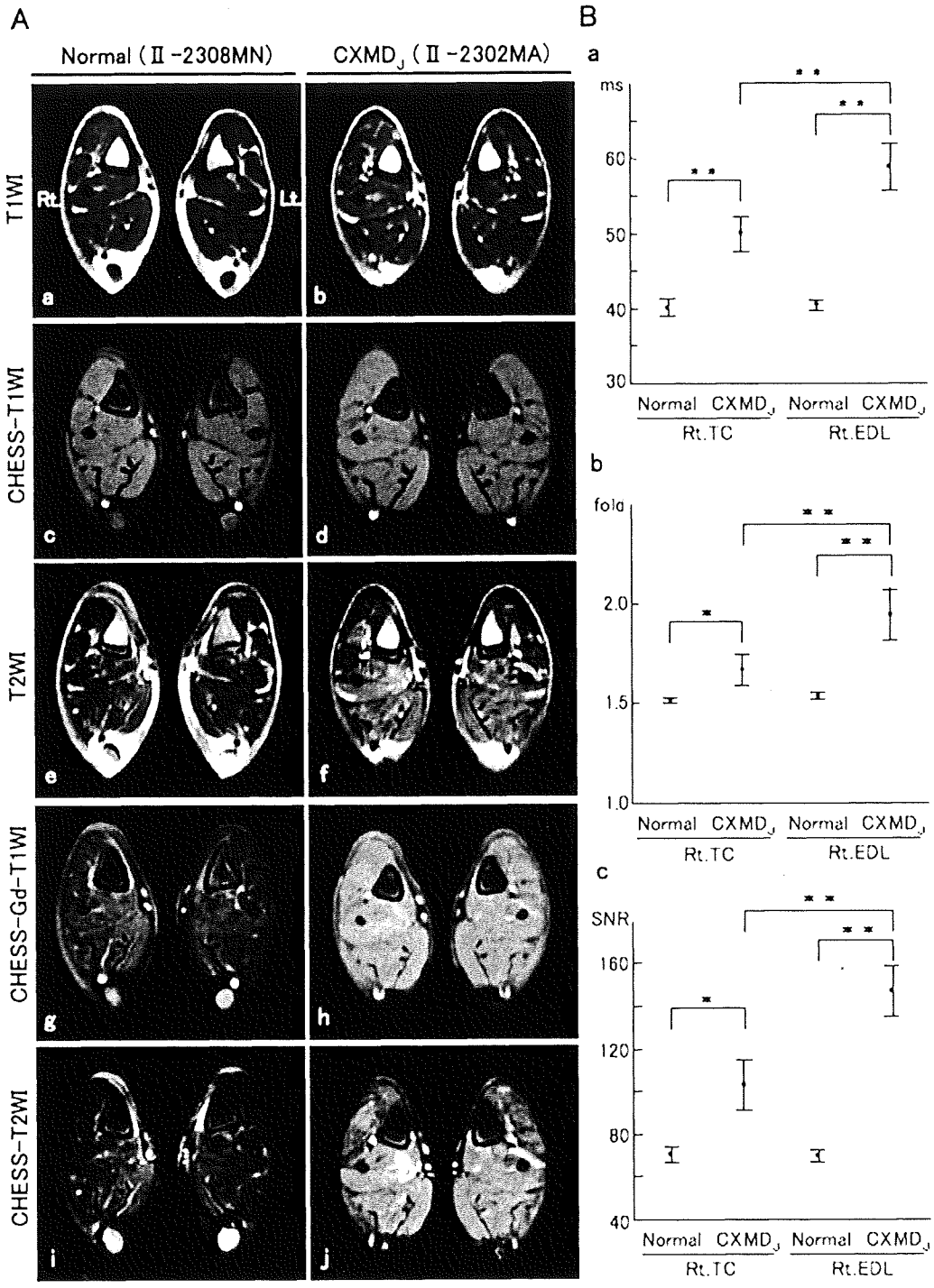

FIGURE 2. Cross-sectional MR images in lower leg muscles of 3-month-old normal and dystrophic dogs and comparison of three quantitative values in Rt. TC and Rt. EDL. **(A)** Representative images of normal (II-2308MN) and dystrophic (II-2302MA) dogs are shown. T1WI **(a, b)**, CHESS-T1WI **(c, d)**, T2WI **(e, f)**, CHESS-Gd-T1WI **(g, h)**, and CHESS-T2WI **(i, j)**. Rt, right side; Lt, left side. **(B)** Comparison of T2 relaxation time **(a)**, contrast enhancement (CE) **(b)**, and SNR of CHESS-T2WI **(c)** between three 3-month-old normal (II-2308MN, II/III-3911MN, and II-4202MN) and three littermate dystrophic (II-2302MA, II/III-3903MA, and II-4204MA) dogs are shown. Rt. TC, right side tibialis cranialis; Rt. EDL, right side extensor digitorum longus. Error bar: mean ± SD; $^{*}P < 0.05$; $^{**}P < 0.01$.

morphological changes of $CXMD_J$ lower leg muscles, we biopsied the Rt. TC and Rt. EDL of a normal dog (II-2308MN) and a $CXMD_J$ dog (II-2302MA) and carried out histopathological examinations. In TC of the $CXMD_J$, we found necrotic fibers, regenerating myofibers with central nuclei, a slight increase in cellular infiltration, and moderate variation in fiber size (Fig. 3A, c). Immunostaining with anti-IgG antibody, which is a marker for muscle necrosis,[37] revealed a slight degree of IgG uptake in the cytoplasm (Fig. 3A, d). On the other hand, EDL of the $CXMD_J$ showed many necrotic and hypercontracted fibers, severe cellular infiltration, and an increase in interstitial connective tissue (Fig. 3B, c). Moreover, the cytoplasm of this muscle showed a severe degree of IgG uptake (Fig. 3B, d). The necrotic and inflammatory changes in the muscle corresponded to the higher SNR on CHESS-T2W images.

MRI Findings of Lower Leg Muscles in a 7-year-old Normal Dog. Next, we obtained muscle images of a 7-year-old normal dog, 00-174MN (Fig. 4A). As shown in Figure 4A, a, c, e, g, and i, the lower leg muscles showed a homogeneous signal intensity in each sequence. Homogeneous but slight contrast enhancement was found on Gd-T1WI and CHESS-Gd-T1WI, as seen in 3-month-old normal dogs.

MRI Findings of Lower Leg Muscles in 7-Year-Old Dystrophic Dogs. We performed muscle MRI on two 7-year-old $CXMD_J$ dogs. II-C04MA showed muscle weakness and atrophy, gait disturbance, macroglossia, arthrogryposis, and dysphagia, but the dog could still rise and walk. Another dog, II-C12MA, was found to have difficulty in rising at the age of about 6.5 years. These two $CXMD_J$ showed mild clinical symptoms and signs despite their ages, which is sometimes seen in less affected GRMD.[8] We have previously reported that the clinical severity in Beagle-crossed dystrophic dogs was milder than that in GRMD,[14] in accordance with a separate report from another facility.[8]

MRI indicated muscle atrophy in both dogs, but the degree of muscle atrophy was more striking in II-C12MA than that in II-C04MA. Figure 4A, b, d, f, h, and j shows representative cross-sectional images of II-C04MA. On T1WI, almost all lower leg muscles of both dogs, in particular TC, EDL, and GC, revealed diffuse hyperintensity regions (Fig. 4A, b), although FHL and FDL did not show remarkable change compared with the normal dog. On CHESS-T1WI, these hyperintense regions were considerably suppressed, suggesting fat infiltration with progression of the disease (Fig. 4A, d), which was reported in a previous MRI study of DMD.[19]

On T2WI, II-C04MA showed slight and moderate hyperintensity in TC and other lower leg muscles, respectively (Fig. 4A, f). On the other hand, II-C12MA also had an area that showed remarkable T2 hyperintensity with T1 hyperintensity, but there is no area of T2 hyperintensity without T1 hyperintensity, with the exception of FHL (data not shown).

On CHESS-T2WI, FDL, GC, FHL, and FDS of II-C04MA and FHL of II-C12MA showed hyperintensity, but significant signal changes were found in neither TC of II-C04MA nor almost all lower leg muscles of II-C12MA (Fig. 4A, j, and data not shown).

On CHESS-Gd-T1WI of II-C04MA, the CHESS sequence considerably suppressed the hyperintense fat signal, but the contrast agent greatly enhanced the muscle regions left in all lower leg muscles, especially EDL, FHL, FDL, GC, and FDS (Fig. 4A, h). Contrast agent uptake was also found on CHESS-Gd-T1WI of II-C12MA, but the degree of uptake was lower than that of II-C04MA (data not shown).

Comparison of MR Signal Intensity in 7-Year-Old Normal and Dystrophic Dogs. To quantitatively assess the MRI findings of $CXMD_J$ dogs, we calculated the T2 relaxation time, CE, and SNR of CHESS-T2WI in TC of one 7-year-old normal dog and two $CXMD_J$ dogs. T2 relaxation time of TC was moderately prolonged in both $CXMD_J$ dogs (46.4 and 47.4 ms) when compared with that in a normal dog (37.0 ms) (Fig. 4B, a). Similarly, the effect of contrast enhancement was also increased in TC of each $CXMD_J$ (1.439- and 1.465-fold) relative to that of a normal dog (1.229-fold) (Fig. 4B, b). However, the SNR of CHESS-T2WI in TC of both $CXMD_J$ dogs (77.7 and 75.0) was not significantly increased when compared with that of a normal dog (74.7) (Fig. 4B, c). The discrepancy between the SNR of CHESS-T2WI and T2 relaxation times, and the effect of contrast enhancement should be carefully considered in the examination of affected skeletal muscle morphology.

Histopathological Findings in Lower Leg Muscles of 7-year-old Normal and Dystrophic Dogs. To determine the relationship between MRI findings and morphological changes in $CXMD_J$ lower leg muscles, we biopsied the Rt. TC of 00-174MN and

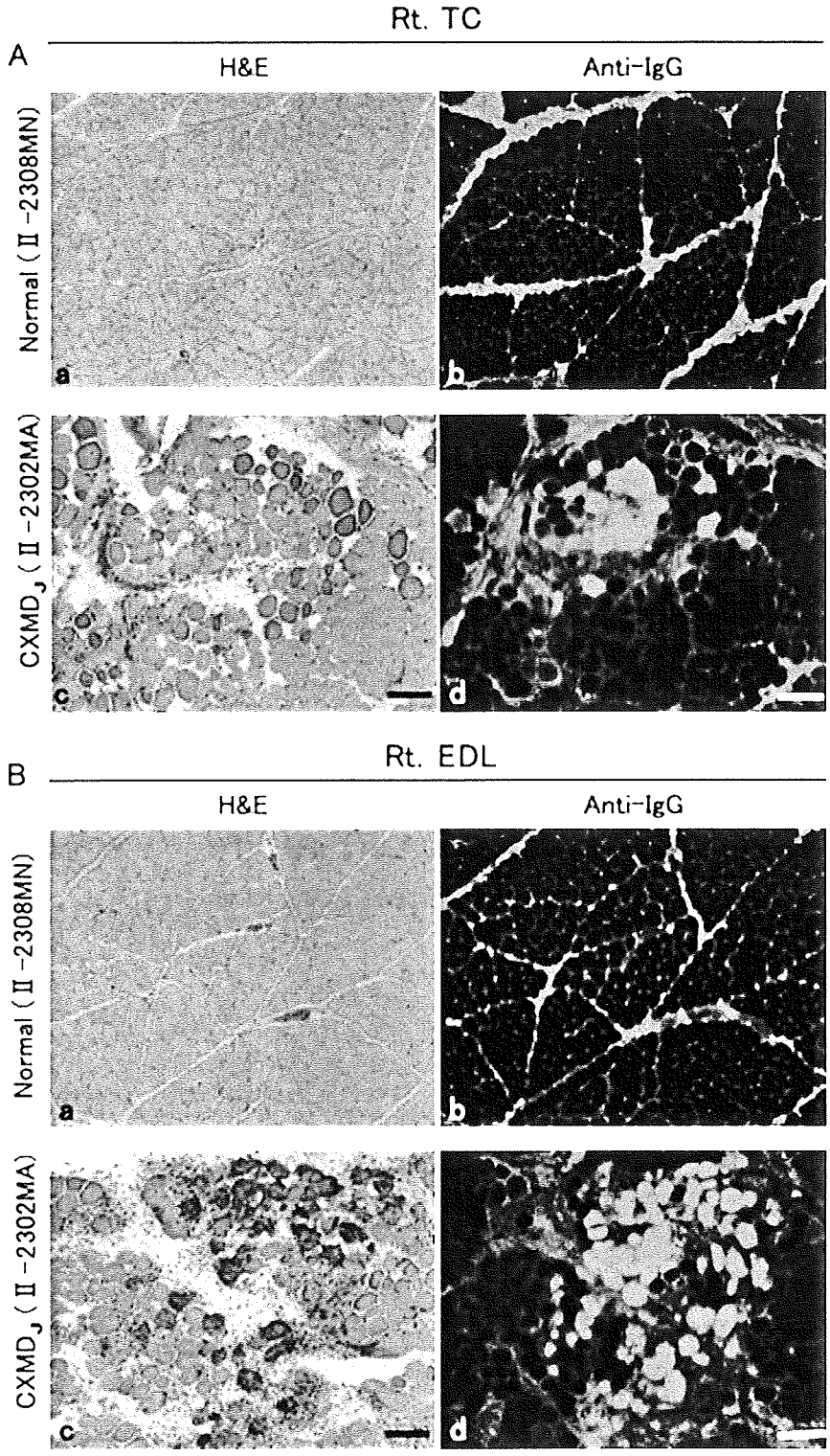

FIGURE 3. Histopathological examinations in Rt. TC and Rt. EDL of 3-month-old normal and dystrophic dogs.**(A)** Hematoxylin and eosin (H&E) staining **(a, c)** and IgG immunostaining **(b, d)** in Rt. TC of 3-month-old normal (II-2308MN) **(a, b)** and dystrophic (II-2302MA) dogs **(c, d)**. **(B)** H&E **(a, c)** and IgG immunostaining **(b, d)** in Rt. EDL of 3-month-old normal (II-2308MN) **(a, b)** and dystrophic (II-2302MA) dogs **(c, d)** are also shown. Bar = 100 μm.

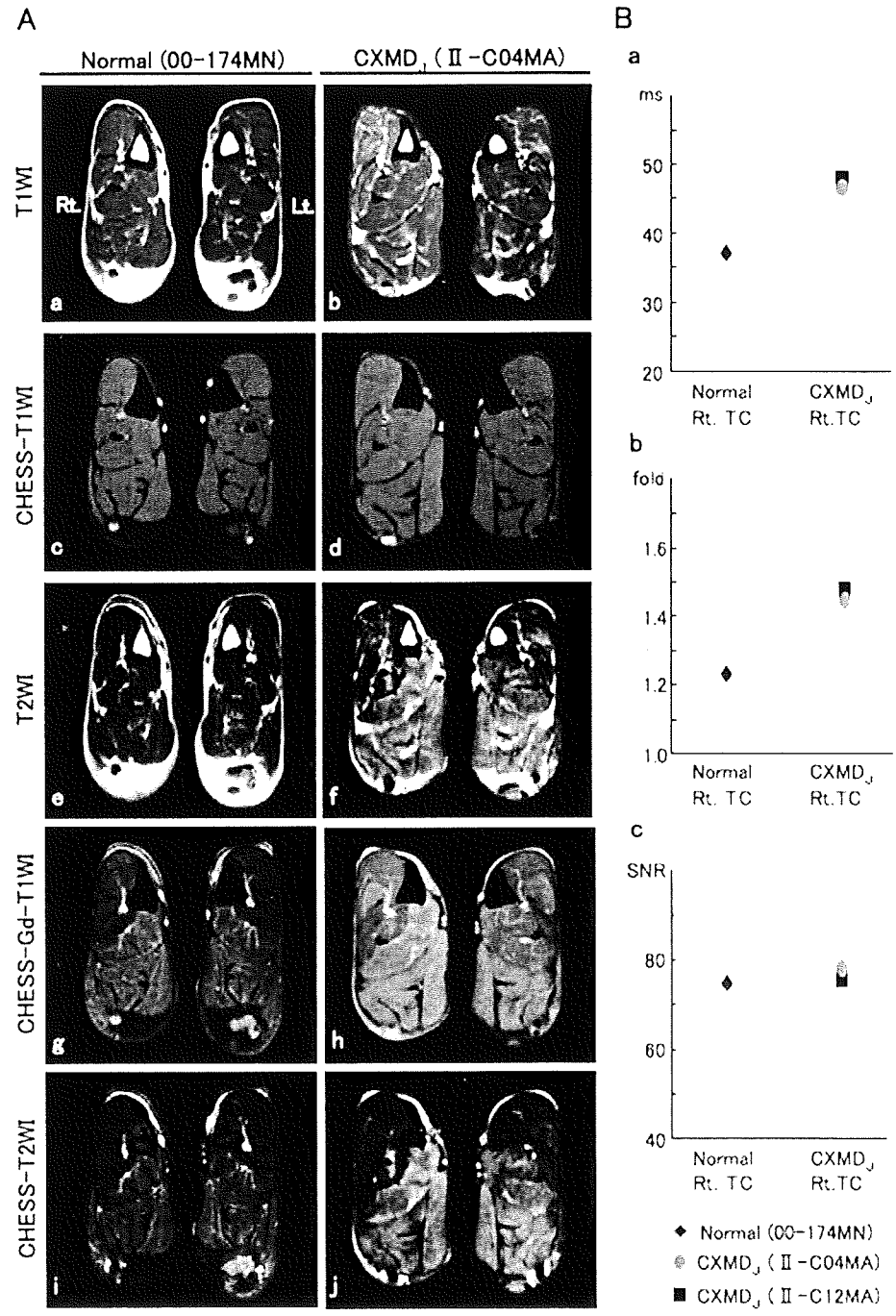

FIGURE 4. Cross-sectional MRI of lower leg muscles of 7-year-old normal and dystrophic dogs and comparison of three quantitative values in Rt. TC. **(A)** Representative images of 7-year-old normal (00-174MN) and dystrophic (II-C04MA) dogs are shown. T1WI **(a, b)**, CHESS-T1WI **(c, d)**, T2WI **(e, f)**, CHESS-Gd-T1WI **(g, h)**, and CHESS-T2WI **(i, j)**. Rt, right side; Lt, left side. **(B)** Comparisons of T2 relaxation time **(a)**, contrast enhancement (CE) **(b)**, and CHESS-T2W SNR **(c)** between the muscles in 7-year-old normal (00-174MN) and dystrophic (II-C04MA and II-C12MA) dogs are shown. TC, tibialis cranialis.

II-C04MA and carried out histopathological examinations. In CXMD$_J$ dogs, we found a few degenerated and many regenerated fibers with central nuclei and a moderate degree of fiber size variation together with fibrotic changes (Fig. 5d). IgG accumulation was found in only a few fibers, but it was extensively distributed in the interstitial tissues (Fig. 5e). Oil red O staining revealed definite fatty infiltration in the CXMD$_J$ dogs (Fig. 5f).

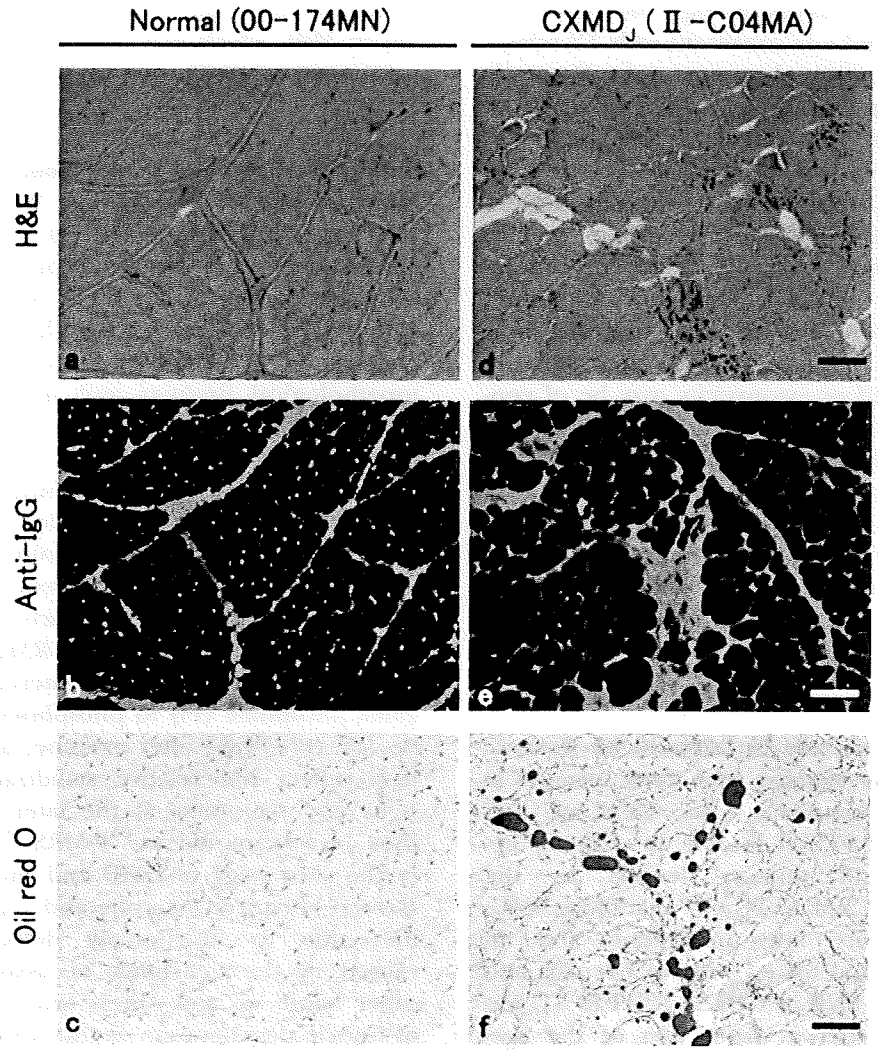

FIGURE 5. Histopathology in Rt. TC of 7-year-old normal and dystrophic dogs. We performed hematoxylin and eosin (H&E) staining **(a, d)**, IgG immunostaining **(b, e)**, and oil red O staining **(c, f)** on tissues of 7-year-old normal (00-174MN) **(a–c)** and dystrophic (II-C04MA) dogs **(d–f)**. Bar = 100 μm.

DISCUSSION

Previous studies have attempted to noninvasively evaluate involvement of striated muscle in DMD patients or the animal models by various MRI sequences; however, a method for more accurate and precise assessment of acute-phase responses such as muscle necrosis and/or inflammation is necessary, because it is difficult to distinguish between these lesions and fat infiltration and/or fibrosis by conventional MRI sequences. Among dystrophic processes, especially in muscle necrosis, the intramuscular water concentration and extracellular components are increased, with the water imbalance having been induced by the deficiency of sarcolemmal membrane integrity.[19,26,38] CHESS-T2WI may be one of the tools to solve this problem, because the sequence can selectively cancel fat tissue signals.

CHESS-T2WI Is Useful to Evaluate Dystrophic Skeletal Muscle Involvement in Early Stage. First, we tried to detect necrotic and/or inflammatory lesions in the early stage of CXMD$_J$ by using a CHESS-T2WI sequence. EDL of a 3-month-old CXMD$_J$ dog showed massive and severe necrosis and inflammatory cell infiltration in the pathological analyses, but TC of the dog revealed localized and moderate necrosis and inflammation. The SNR of CHESS-T2WI in EDL showed a significant increase compared with that in TC. These findings suggest that there is a correlation between SNR of CHESS-T2WI and the degree of necrotic and inflamma-

tory changes in the histopathology. Moreover, the SNR of CHESS-T2WI was consistent with T2 relaxation time or contrast enhancement in the early stage of muscular dystrophy. Previous contrast agent studies sensitively detected early dystrophic muscle involvement that showed the increase of cell membrane permeability.[24,25] In the forelegs of 2-month-old GRMD dogs, the maximum relative enhancement, which was calculated from fat-saturated T1-weighted images pre- and post-gadolinium injection, was almost doubled compared with normal control dogs.[39] However, side effects of the contrast agent itself or cytotoxicity may be of concern, because influx of the contrast agent into damaged muscle fibers occurred. CHESS-T2WI can identify dystrophic lesions without a contrast agent and may facilitate more sensitive and clearer optical evaluation of early dystrophic lesions than other fat suppression sequences, because the SNR on either STIR or the multipoint Dixon technique is lower than that on CHESS.[40]

CHESS-T2WI May Be Able to Differentiate Necrotic and/or Inflammatory Changes from Fatty Changes in Advanced Stage of Dystrophic Dogs. Next, we studied whether CHESS-T2WI is able to evaluate necrotic and/or inflammatory lesions in the advanced stage of $CXMD_J$. TC of 7-year-old $CXMD_J$ dogs showed severe fatty infiltration and an increase in interstitial tissues without necrosis and inflammation. The SNR of CHESS-T2WI in TC was not significantly different from that of the age-matched normal dog, suggesting that CHESS-T2WI is a good tool to evaluate necrotic and/or inflammatory changes, even though extensive fatty infiltration exists. On the other hand, the T2 relaxation time and enhancing effect of the contrast agent were increased, although necrotic and inflammatory changes were not present. It is possible that the prolongation of T2 relaxation time or the increase of contrast enhancement is affected by fatty infiltration, increase of interstitium, and/or microvascular flow, and therefore necrotic and inflammatory changes could be overestimated by these sequences and indexes. CHESS-T2WI may reflect necrotic lesions more precisely in the intermediate to advanced stage without special contrast agents, because the SNR of CHESS-T2WI was elevated in EDL of II-C04MA, where it is thought that necrotic and fatty changes coexist (data not shown). On the other hand, it is also important to evaluate fatty infiltration in the advanced stages of DMD. In a recent study, the percentage of intramuscular fat tissue was measured by three-point Dixon MRI, which may accurately reflect the clinical severity of DMD patients.[41]

Muscle Regeneration in Advanced Stage of $CXMD_J$ May Stabilize Cell Membrane. We found that the majority of muscle fibers in TC of 7-year-old $CXMD_J$ dogs were composed of regenerated fibers with central nuclei, but those fibers did not show IgG uptake, in accordance with the lack of abnormal signals on CHESS-T2WI at this stage. The histopathological findings and muscle physiological functions were ameliorated at the advanced stage in *mdx* mice compared with those in the early stage.[9] Moreover, studies using 31-phosphorus magnetic resonance spectroscopy (^{31}P-MRS) demonstrated biochemical abnormalities in the regulations of intracellular ion and oxidative metabolism of dystrophic muscles at the early stage.[42–45] It was, however, reported that older GRMD (>30 months) did not demonstrate further increases in the inorganic phosphate (Pi) to phosphocreatine (PCr) ratio [Pi/(Pi+PCr)] after exercise, and these results may reflect the relative stabilization of clinical signs and symptoms at the later stage, as far as they were examined by ^{31}P-MRS.[45] Skeletal muscle in the early stage of DMD and the model animals showed enhanced necrotic and regeneration activities due to functionally defective regulation caused by the deficiency of dystrophin. On the other hand, we and others found a lower degree of muscle degeneration at the advanced stage, suggesting some degree of membrane stability remains in regenerated fibers, resulting in resistance to further necrosis. Retention of membrane stability in the advanced stage may be related to the shift of muscle fiber types from fast to slow[46] and/or compensatory expression of utrophin,[47] a homolog of dystrophin.

One of the limitations of the CHESS sequence is that it requires a presaturation pulse. Fat suppression by the CHESS sequence is not applicable with a low magnetic field (<1.5 T), because dispersion of the frequency direction between water and fat depends on the main magnetic field.[48] Another limitation is that CHESS-T2WI does not allow evaluation of fibrotic changes. We, however, suggest that CHESS-T2WI could precisely and perceptively provide much information, such as the presence and severity of necrotic and inflammatory changes throughout all stages of the disease. Moreover, CHESS-T2WI is safer than other conventional sequences, because the sequence does not require